PCCP

Accepted Manuscript

ROYAL SOCIETY OF CHEMISTRY

www.rsc.org/pccp

Journal Name

ARTICLE

Understanding Molecular Switching Properties of Octaphyrins

Received 00th January 20xx,
Accepted 00th January 20xx

DOI: 10.1039/x0xx00000x

www.rsc.org/

T. Woller,[a] J. Contreras-García,[b] P. Geerlings,[a] Frank De Proft,[a] and M. Alonso[a*]

Several expanded porphyrins switch between Hückel, Möbius and twisted-Hückel topologies, encoding different aromaticity and NLO properties. Since the topological switch can be induced by different external *stimuli*, expanded porphyrins represent a promising platform to develop molecular switches for molecular electronic devices. In order to determine the optimum conditions for efficient molecular switches from octaphyrins, we have carried out a comprehensive quantum chemical study focused on the conformational preferences and aromaticity of [36]octaphyrins. Different external *stimuli* for triggering the topological switch have been considered in our work, such as protonation and redox reactions. Importantly, the structure-property relationships between the molecular conformation, number of π-electrons and aromaticity in octaphyrins have been established by using energetic, magnetic, structural and reactivity descriptors. Importantly, we found that the aromaticity of octaphyrins is highly dependent on the π-conjugation topology and the number of π-electrons and it can be modulated by protonation and redox reactions. A non-aromatic figure-eight conformation is strongly preferred by neutral [36]octaphyrins, that switches to a Möbius aromatic conformation upon protonation. Such a change of topology involves an aromaticity switch in a single molecule and is accompanied by a drastic change in the NLO properties. By contrast, the twisted-Hückel topology remains the most stable one in the oxidized and reduced species, but the aromaticity is totally reverse upon redox reactions. Aromaticity is shown to be a key concept in expanded porphyrins, determining the electronic, magnetic and NLO properties of these macrocycles.

Introduction

Hückel's rule has long been a cornerstone of aromaticity for monocycles that fulfil specific electronic and structural features.[1] According to Hückel's rule, aromatic systems present a full cyclic electron delocalization, conformational planarity and contain [4*n* + 2] π-electrons in their conjugation pathway. By contrast, cyclic molecules with [4*n*] π-electrons such as cyclooctatetraene are antiaromatic on the basis of Hückel's rule. However, Hückel´s rule was originally derived for monocyclic systems containing identical atoms, so this rule cannot be strictly applied to porphyrinoids that contain multiple heterocyclic rings. In the last decade, the concept of aromaticity has been expanded to organometallic and inorganic species,[2] all-metal clusters,[3] nanomaterials[4] and non-planar compounds.[5] As a consequence of the proliferation of new aromatic compounds, the concept of aromaticity had to be refined and new types of aromaticity emerged, such as Möbius aromaticity.[6]

The intriguing concept of Möbius aromaticity predicts that [4*n*]annulenes with a twisted Möbius-strip topology are aromatic.[7] Although the concept of Möbius aromaticity was proposed by Heilbronner in 1964, the first singly-twisted Möbius annulene was not synthesized until 2003.[8] In recent years, expanded porphyrins have emerged as a very effective platform to realize Möbius aromatic molecules aided by metal coordination, solvent, N-fusion reactions or protonation.[9] These systems have definite advantages in the formation of Möbius aromatic molecules such as overall conformational flexibility, ability to invert the pyrrolic subunits under certain conditions, multiple oxidation states, which can be easily interconverted by two-electron redox reactions, and possibility of "locking in" Möbius conformations through metalation by the formation of both N-metal and C-metal bonds.[10]

Besides the Möbius topology, expanded porphyrins can adopt a variety of conformations with Hückel and twisted-Hückel topologies that can be interconverted under certain conditions.[11] Interestingly, the photophysical and nonlinear optical (NLO) properties of expanded porphyrins strongly depend on the macrocyclic aromaticity of the π-electron system and the molecular topology, as proven by several experimental and theoretical studies.[12,13]

For all the reasons mentioned above, expanded porphyrins provide a test bed in which the concept of aromaticity can be explored.[14] Depending on the topology of the π-conjugated system, the validity of the Hückel´s rule and the Möbius aromaticity in heteroannulenes can be assessed. In principle, π-conjugated systems with an even number of half-twists (or, more precisely, with an even linking number L_k)[15] should follow

[a] Eenheid Algemene Chemie (ALGC), Vrije Universiteit Brussel (VUB). Pleinlaan 2, 1050 Brussels (Belgium).
[b] Laboratoire de Chimie Théorique, 4 Pl. Jussieu, 75252 Paris cedex 05 (France).

Electronic Supplementary Information (ESI) available: DFT benchmark study, comparison between the B3LYP and M06 relative energies, torsional descriptors and bond-length alternation parameters of the different conformations of octaphyrins, ^{1}H NMR chemical shifts of *meso*-octakis(pentafluorophenyl) octaphyrins, relationships between aromaticity indices and M06/6-31G(d,p)-optimized geometries. See DOI: 10.1039/x0xx00000x

the Hückel's rule, while those with an odd number of half-twists (odd values for L_k) follow the Möbius aromaticity.

Nevertheless, the quantification of aromaticity in expanded porphyrins is difficult. Aromaticity is currently described as a multidimensional phenomenon, implying that the aromatic character cannot be quantified using a single aromaticity descriptor.[16] In fact, the aromaticity of porphyrinoids was shown to be particularly "multifaceted", resulting in large discrepancies between energetic and magnetic descriptors.[17] Consequently, many authors suggest using several descriptors of aromaticity based on different criteria. In previous works, we proposed a set of aromaticity descriptors based on energetic, structural, magnetic and reactivity criteria.[18,19] By using these descriptors, the structure-property relationships between the molecular conformations, the number of π-electrons and aromaticity was established and the optimum conditions for viable Möbius expanded porphyrins were determined for pentaphyrins,[20] hexaphyrins[18] and heptaphyrins.[21]

Through extensive density functional theory calculations, we demonstrated that the molecular topology is highly influenced by the number of π-electrons and the size of the macrocycle. [4*n* + 2] π-electron expanded porphyrins adopt Hückel conformations, almost planar and highly aromatic whereas antiaromatic Hückel and Möbius conformers coexist in dynamic equilibrium for [4*n*] π-electrons expanded porphyrins.[18,20] The larger [32]heptaphyrin strongly prefers a figure-eight conformation in the neutral state, but the Möbius topology became the most stable in protonated species.[21] Alternatively, conformational control in most of these expanded porphyrins can be achieved by changing the *meso*-substituents.[20,21]

Remarkably, Hückel-Möbius topological switches were found to be feasible in [4*n*] π-electron expanded porphyrins, such as [28]hexaphyrin[18] and [32]heptaphyrin.[21] These expanded porphyrins are able to switch between distinct π-conjugation topologies, encoding different photophysical and NLO properties.[22] The topological switch can be induced by protonation,[23] solvation[24] and redox agents[25] and involves aromaticity switching in a single molecule. These features make expanded porphyrins suitable for the development of a novel type of molecular switches for nanoelectronic applications.

In order to expand our research toward the design of functional molecular switches from expanded porphyrins, we examined the different factors involved in the switching process of [36]octaphyrin(1.1.1.1.1.1.1.1). Octaphyrin macrocycles contain 8 pyrrole rings connected via *meso*-carbon bridges. This class of expanded porphyrins exhibit interesting properties such as multi-metal coordination,[26] dynamic structures,[11] and facile redox reactions.[27] Appealingly, [36]octaphyrin provides Möbius aromatic structures upon protonation leading to large variations in the NLO properties.[28]

Using DFT calculations, the conformational preferences of [36]octaphyrins in both gas-phase and several solvents has been thoroughly investigated (Scheme 1). Moreover, we have analysed the influence of *meso*- and *β*-substituents on the stability of the figure-eight, Möbius and Hückel conformations. Then, we intend to determine effective external *stimuli* for triggering topological/aromaticity switches in octaphyrins. In this sense, the ability of redox reactions and protonation to induce conformational and/or π-electron switching in octaphyrins has been investigated. Once the conformational control in octaphyrins is fully understood, the aromaticity of the twisted-Hückel, Möbius and Hückel conformers with different oxidation and protonation state has been quantified using energetic, magnetic, structural and reactivity criteria. Importantly, the structure-property relationships between molecular topology, aromaticity and NLO properties have been established. Identifying methods to properly quantify the aromaticity of these unique macrocycles systems might help in the design of octaphyrins with optimal and specific properties.

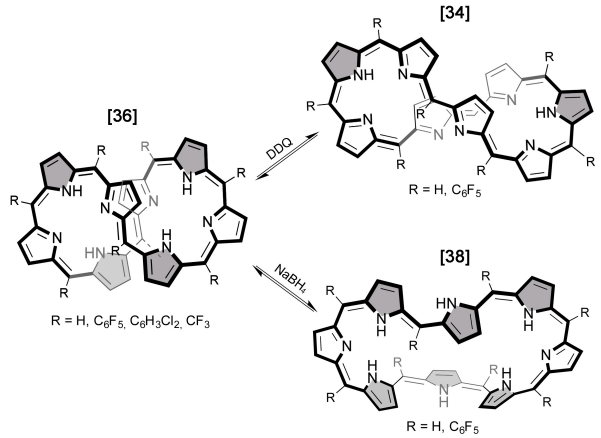

Scheme 1 Molecular structures of [36]octaphyrins and their redox- triggered interconversions leading to [34] and [38]octaphyrins.

Computational details

All the calculations were performed with the Gaussian 09 program package[29] using the M06 functional[30] together with split-valence basis sets [6-31G(d,p) and 6-311G(d,p)].[31] In our benchmark study, the M06 functional was proven to be the most accurate in reproducing the crystallographic structure of various Hückel and Möbius [36]octaphyrins. The geometries of the different conformations of neutral and diprotonated octaphyrins were fully optimized and characterized by harmonic-vibrational-frequency computations at the M06/6-31G(d,p) level of theory. All the structures were found to correspond to minima on the potential energy surface with no imaginary frequencies. Then, single point calculations using the triple-ζ-quality 6-311+G(d,p) basis set were performed in order to compute more accurate electronic energies in both gas-phase and several solvents. Implicit solvent effects were taken into account by using the polarizable continuum model (PCM) with radii and non-electrostatic terms from the SMD model of Truhlar and co-workers.[32]

The harmonic oscillator model of aromaticity (HOMA), defined by Kruszewski and Krygowski [Eq. (1)], was computed as a structural descriptor of aromaticity.[33]

$$\mathrm{HOMA} = 1 - \frac{\alpha}{n}\sum_{i=1}(R_{opt} - R_i)^2 \quad (1)$$

Where α is an empirical constant fixed for each type of bond and *n* corresponds to the number of bonds taken into account in the summation. Consequently, HOMA equals 0 for non-aromatic systems whereas HOMA=1 for fully aromatic ones with all bonds equal to the optimal value R_{opt}. R_i denotes the running bond length along the annulene-type conjugation pathway.[34]

The isomerization method[19] was applied to evaluate the isomerization stabilization energies (ISE), magnetic susceptibility exaltation[35] (Λ) and relative hardness[36] ($\Delta\eta$) of octaphyrins. The reactions that were used to compute the aromaticity indices of the twisted-Hückel and Hückel octaphyrins with [36] and [38] π-electrons are shown in Scheme 2.

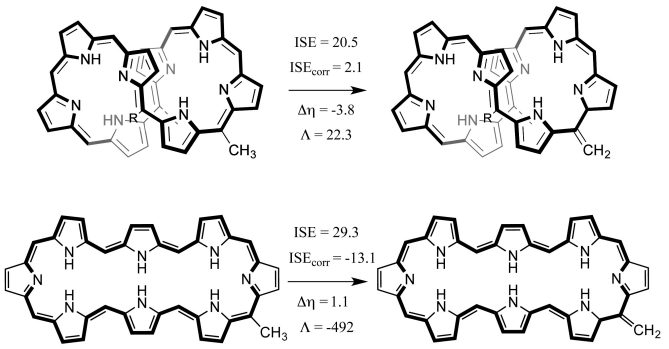

Scheme 2 Reaction used to evaluate several aromaticity descriptors in octaphyrins. ISE and Δη are given in kcal mol^{-1} and Λ in ppm cgs.

The *syn-anti* corrections for the isomerization stabilization energies were evaluated as the energy difference between the dihydrogen derivative of the *meso*-methyl octaphyrin and its respective nonaromatic isomer (Scheme S1). Magnetic susceptibilities were computed by employing the CSGT method[37] at the B3LYP/6-31+G(d,p) level of theory and the GIAO[38]/B3LYP/6-311+G(d,p) method was applied for the NICS (nucleus-independent chemical shift) calculations.[39] NICS values were computed at the geometrical center of the 36 heavy atoms of the octaphyrin framework [NICS(0)] and at 1 Å above the ring center [NICS(1)]. The ^{1}H magnetic shielding tensors were computed with the GIAO method at the B3LYP/6-311+G(d,p) level in the solvent used experimentally. To compare isotropic shieldings with the experimentally observed chemical shifts, the NMR parameters for TMS were calculated at the same level and used as the reference molecule. The HOMO and LUMO energies were used for computing the hardness (η) of the methyl and methylene isomers involved in the isomerization reaction.

As a torsional strain descriptor (Φ_p), we used the average dihedral angle between neighboring pyrrole rings, whereas the extent of the effective overlap of neighboring *p*-orbitals was quantified through the torsional π-conjugation index (Π), defined as follows:[11]

$$\Pi = \prod_i \cos\varphi_i \quad (2)$$

where φ_i are the dihedral angles along the classical conjugation pathway (CP). Π equals 1 for a completely planar system, it is positive for any Hückel (double-sided) conformation and negative for any Möbius (single-sided) surface. Normally, macrocyclic aromaticity is associated with porphyrinoids having Π values higher than 0.3.[11]

The hydrogen bonding inside the different macrocycles was evaluated with two different methods. The hydrogen-bond index (N_H) roughly indicates the number of intramolecular hydrogen bonds stabilizing the conformation and assigns a value of 1 for single N-H···N bonds and 1.5 for bifurcated ones. Besides, the semi-quantitative noncovalent interaction (NCI) index was used to evaluate the strength and number of hydrogen bonds.[40] For the NCI analysis, the wave function files of the optimized geometries at the M06/6-31G(d,p) level of theory were used as an input in the NCIPLOT v.1.0 program.[41]

Results and discussion

DFT benchmark study for Hückel and Möbius octaphyrins

First, the performance of several exchange-correlation functionals (B3LYP,[42] PBE,[43] M06,[30] ωB97XD,[44] B3LYP-D[45] and BP86[46]) in reproducing the molecular structure of various *meso*-substituted octaphyrins was assessed by comparison with the X-ray diffraction data. To this end, we have chosen the neutral and diprotonated *meso*-octakis(pentafluorophenyl) [36]octaphyrins with a twisted-Hückel topology and a Möbius topology, respectively (Figure S1).[27,28] In this benchmark study, the comparison criteria were based on the root-mean-square deviation (RMS) between DFT-optimized and the X-ray Cartesian coordinates as well as the mean unsigned error (MUE) between interatomic distances and dihedral angles (Tables S1-S4).

According to the RMS values, the hybrid meta functional M06 clearly outperforms the "standard" functionals not including dispersion (B3LYP, PBE and BP86) and the long-range corrected hybrid functional ωB97XD in the description of the figure-eight conformation of the neutral [36]octaphyrin (Fig. 1). However, the degree of bond alternation along the conjugation pathway is better reproduced by the standard functionals such as PBE. The HOMA of the crystallographic structure is 0.68 compared to 0.74 (M06), 0.70 (B3LYP), 0.69 (PBE), 0.67 (BP86) and 0.59 (ωB97XD). So, M06 slightly overestimates the degree of π-electron delocalization of the figure-eight conformation, whereas ωB97XD predicts a more bond-alternating geometry.

In the case of the Möbius diprotonated [36]octaphyrin, M06 and ωB97XD functionals present the best and the worst overall performance for describing the geometry of the singly-twisted topology (Fig. S3). However, the degree of bond-alternation ($HOMA_{RX}$ = 0.72) is better described by the M06-optimized geometries (HOMA = 0.70), followed by the B3LYP-optimized ones (HOMA = 0.75). Again, the ωB97XD functional underestimates degree of π-electron delocalization, predicting a Möbius structure with HOMA = 0.58.

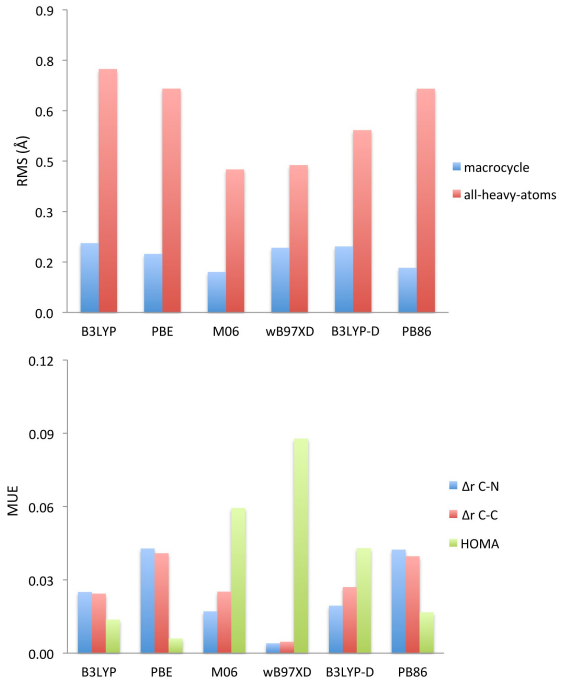

Fig. 1 (a) Root-mean-square deviations (RMS) and (b) mean unsigned errors (MUE) for the bond-length alternation parameters of the DFT optimized geometries relative to the X-ray structure of the neutral *meso*-octakis(pentafluorophenyl) [36]octaphyrin.

Recently, we found that the π-π stacking interactions in the figure-eight heptaphyrins are overemphasized in functionals that account for dispersion, especially M06-2X.[21] Accordingly, we have performed a geometrical analysis of the different types of π-π stacking interactions present in the twisted-Hückel topology: pyrrole-pyrrole, C_6F_5-C_6F_5 and C_6F_5-pyrrole (Table S5). In contrast to M06-2X with double amount of HF exchange, the M06 functional provides the most accurate description of the different π-π stacking interactions. Only, the centroid-centroid distance between the stacked pyrrole rings is reduced from 3.41 Å in the X-ray structure to 3.33 Å with M06. On the contrary, the worst evaluation of the stacking interactions is observed in the B3LYP-optimized structures, in which the distances between the stacked rings are significantly increased.

In summary, the M06 hybrid functional presents the best overall performance in describing the geometries of the Hückel and Möbius topologies of the [36]octaphyrin. The worst performance is observed for the ωB97XD functional, which underestimates the degree of bond equalization in octaphyrins. The widely used B3LYP functional describes the overall structures worse, but performs very well for describing the degree of bond-alternation. Therefore, the conformational analysis of neutral unsubstituted [36]octaphyrin will be performed using the M06 functional.

Conformational analysis of neutral unsubstituted [36]octaphyrin

Given the large amount of possible conformers for octaphyrins, we initially investigated eight conformers for which the crystallographic structure was available (Fig. 2). These conformations were observed experimentally for all-aza octaphyrins varying in oxidation state, protonation and metalation.[11] Besides, 5 new conformations (**d**, **j**-**m**) were found in the analysis of the interconversion pathways between the different conformers and they were also included in the conformational analysis of neutral unsubstituted [36]octaphyrin **1**. The different conformations are described by the topological descriptors Tn^X, which indicates the number of half-twists (*n*) and the subunits located between two *transoid* linkages (^{X}). In addition, Hückel and Möbius topologies can be distinguished by counting the number of formal *trans* bonds in the smallest macrocyclic pathway. The conformation has a Möbius topology (*T1*, *T3*, etc.) when the number of *trans* bonds is odd. On the contrary, Hückel conformers contain an even number of *trans* bonds.[11] The 13 conformers can be classified into four different π-conjugation topologies: untwisted Hückel (*T0*), singly-twisted Möbius (*T1*), twisted-Hückel (*T2*) and triply-twisted Möbius (*T3*) topologies. Although there is not any experimental evidence for the latter conformer, a similar triply-twisted Möbius conformation was recently identified in decaphyrins[47] and annulennes.[48]

Since solvent can induce a change of topology in certain expanded porphyrins,[24] we have also investigated the solvation effects in the conformational relative energies of neutral unsubstituted [36]octaphyrin **1** using the SMD model.[32] The relative energies of the different conformations in gas-phase, dimethylsulfoxide (DMSO), dichloromethane (DCM) and tetrahydrofuran (THF) together with the hydrogen bonding index (N_H) and ring strain (Φ_p) are collected in Table 1.

Table 1. Relative energies and relative Gibbs free energies (in kcal mol^{-1}) in gas-phase and different solvents together with the hydrogen bonding index (N_H) and ring strain (Φ_p in °) of the different conformations of neutral unsubstituted [36]octaphyrin **1**.[a]

conf	Tn^X	E_{rel}	ΔG_{298}	N_H	Φ_p	ΔG_{THF}	ΔG_{DCM}	ΔG_{DMSO}
1a	$T0^{5,10,25,30}$	23.3	20.0	3	13.0	13.2	12.2	12.1
1b	$T0^{B,C,E,F,H}$	43.7	41.3	0	16.9	47.3	45.7	44.8
1c	$T0^{B,F,5,20,25}$	26.8	25.5	3	23.6	22.4	21.8	22.6
1d	$T0^{B,F,20,25}$	32.0	31.4	3	27.3	28.6	28.0	28.3
1e	$T1^{B,C,E,H}$	47.1	45.0	0	30.3	40.1	38.7	38.4
1f	$T1^{B,C,F}$	26.6	25.4	2.5	31.5	17.9	17.0	16.7
1g	$T2^{B,F}$	17.3	17.3	3	18.4	12.5	12.0	11.3
1h	$T2^{C,G}$	16.3	15.5	3	15.0	11.3	10.8	10.4
1i	$T2_{RX}$	0.0	0.0	4	15.0	0.0	0.0	0.0
1j	*T3*	26.9	26.5	3	31.5	31.5	24.9	24.4
1k	$T0^{B,C,E,G}$	43.9	41.8	1	16.9	16.9	35.2	33.9
1l	$T1^{B,C,E,G}$	46.9	45.2	1	33.9	33.9	38.3	37.0
1m	$T2^{B}$	11.0	10.6	3.5	16.3	16.3	9.2	8.9

[a] ZPE-corrected relative energies and Gibbs free energies at the M06/6-311+G(d,p)//M06/6-31G(d,p) level of theory.

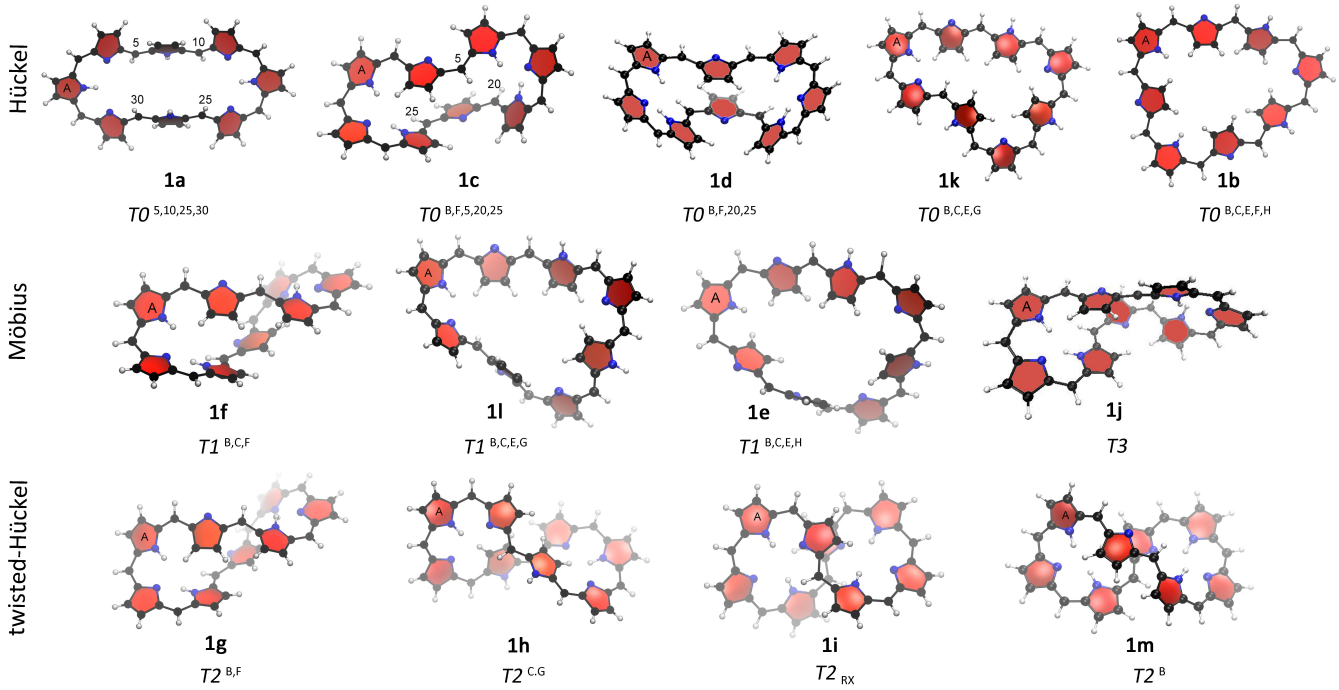

Fig. 2 Hückel, Möbius and twisted-Hückel conformations of neutral unsubstituted [36]octaphyrin **1** (**a**-**m**).

Despite its expected antiaromatic behaviour according to Hückel´s rule, the figure-eight conformation $T2_{RX}$ (**1i**) is the global minimum for the neutral unsubstituted [36]octaphyrin **1**, both in gas phase and in solvent. This conformational preference results from the effective intramolecular hydrogen bond network and the lower ring strain of the structure **1i**. In addition, we observed that the two hemi-porphyrins-like segments of **1i** are roughly parallel and planar with an interplanar distance of 3.3 Å, which is close to the distance of π–π stacking interaction. Owing to higher ring strain and fewer hydrogen bonds, the Möbius and untwisted Hückel topology are 20-45 kcal mol^{-1} higher in energy than the global minimum **1i**.

Even though the figure-eight conformation **1i** is predominant in all the tested solvents and gas-phase, several Hückel and Möbius topologies are further stabilized in polar solvents. Generally, the solvent effects are more pronounced in conformations with outward-pointing pyrrole rings, such as **1a** and **1f**. In both cases, polar solvents reduce their Gibbs free energy by more than 7 kcal mol^{-1}. This stabilization is related to the formation of intermolecular hydrogen bonds between the outward-pointing NH groups and the solvent molecules. The solvent effects are less important for the twisted-Hückel topologies, especially the $T2_{RX}$, in which all pyrrolic nitrogens are pointing inward the macrocycle. Therefore, the conformational equilibrium in [36]octaphyrin is displaced in polar solvents towards more extended conformations with inverted pyrrole rings.

In analogy with other [4*n*] π-electrons expanded porphyrins,[21,49] the conformational stability of unsubstituted [36]octaphyrins is governed by the number and the strength of intramolecular hydrogen bonding (Fig. 3). The correlation between the relative stabilities and the N_H values of the different conformations is high and the slope of the regression line is 9.9. That means that one intramolecular hydrogen bond affords stabilization by about 10 kcal mol^{-1} in neutral [36]octaphyrin. Remarkably, a similar stabilization effect by *ca.* 10 kcal mol^{-1} per N_H was previously reported for [28]hexaphyrin[49] and [32]heptaphyrin.[21]

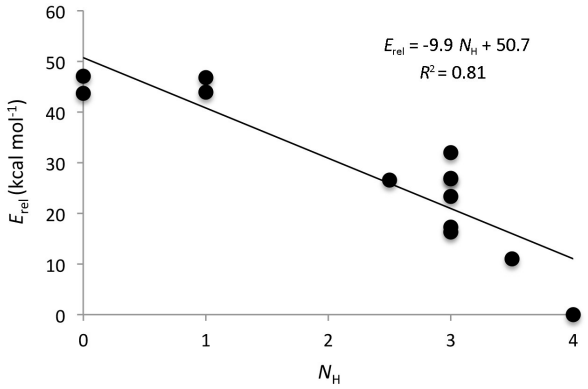

Fig. 3 Relationship between the relative energy of neutral [36]octaphyrin conformers (**1a**-**m**) and the hydrogen bonding index (N_H).

By contrast, the ring strain does not play a major role in the conformational stability of neutral unsubstituted [36]octaphyrins (Fig. S8). For instance, despite having a lower ring strain, the conformational energy of **1a** is 20 kcal mol^{-1} above **1i**. However, the instability of Möbius topologies could be related to their higher ring strain compared to twisted-Hückel topologies. Furthermore, the Möbius topologies of the neutral unsubstituted [36]octaphyrins present a less effective π-conjugation overlap (-0.35 < Π < -0.57) than twisted-Hückel topologies (0.64 < Π < 0.80). This less effective π-conjugation is

Journal Name

ARTICLE

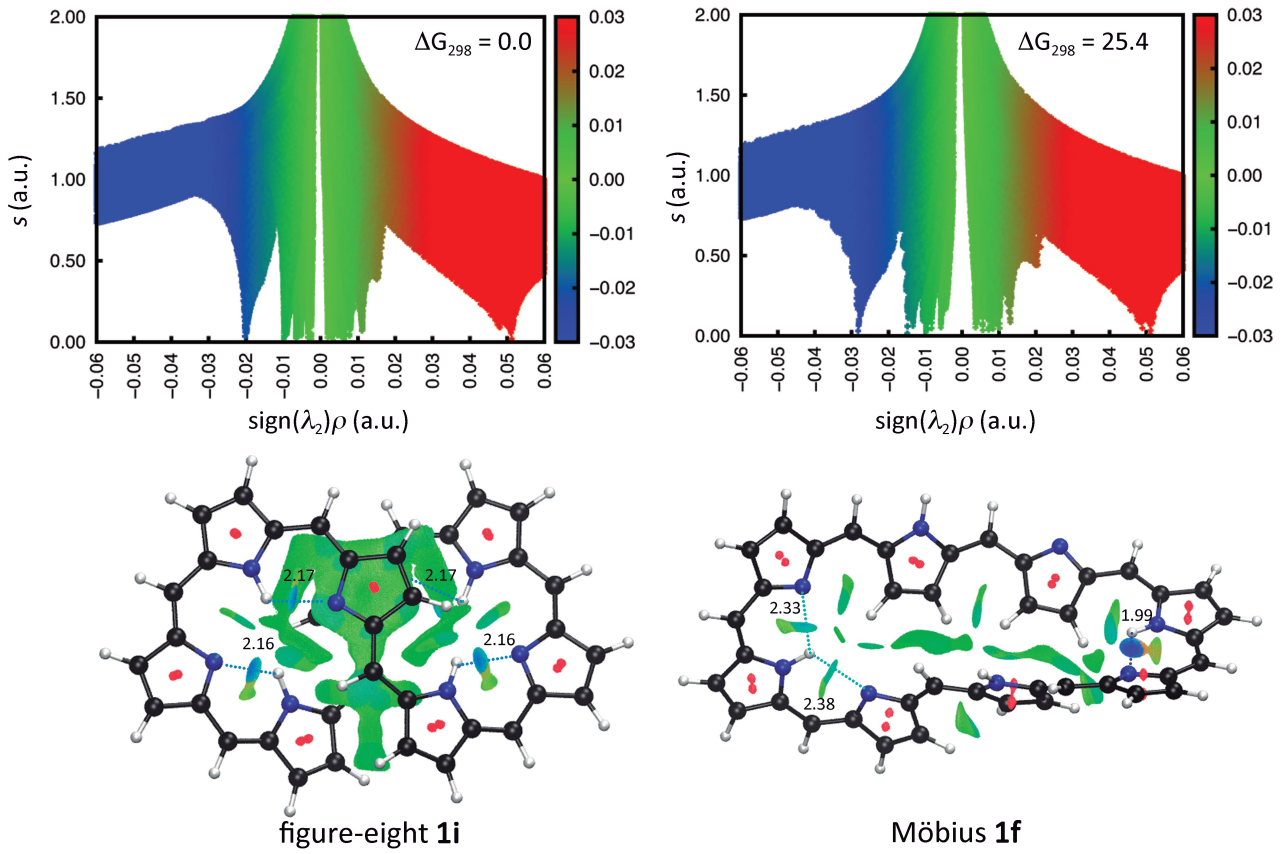

Fig. 4 NCI analysis of the doubly and singly twisted topologies of neutral unsubstituted [36]octaphyrin **1**. Plots of the reduced density gradient $s(\rho)$ and gradient isosurfaces (s = 0.5). The surfaces are coloured according to sign(λ_2)ρ over the range -0.03 to 0.03 a.u. The hydrogen bond lengths (in Å) are also shown.

correlated to the larger dihedral angles along the conjugation pathway and thus the larger ring strain.

The role of non-covalent interactions in determining the conformational preferences of neutral [36]octaphyrins was also scrutinized by the non-covalent interaction (NCI) method.[40] The NCI method characterizes non-covalent interactions using the electron density and its first derivative. In this method, the sign of the second eigenvalue λ_2 enables to distinguish attractive ($\lambda_2 < 0$) from repulsive interactions ($\lambda_2 > 0$) whereas the magnitude of the density itself indicates the strength of the interaction. Weak van der Waals interactions are characterized by values of sign(λ_2)ρ close to 0 whereas stronger hydrogen bonds appear in the region of -0.015 to -0.04 a.u.[50]

Fig. 4 illustrates the computed $s(\rho)$ diagrams and NCI isosurfaces for the twisted-Hückel **1a** and Möbius **1f** conformers of neutral [36]octaphyrin. Apart from the repulsive interaction at the center of each pyrrole ring, both conformations differ in the number and type of non-covalent interactions. The figure-eight topology **1i** is stabilized by four single hydrogen bonds whereas one bifurcated and one single hydrogen bond are encountered in the Möbius topology **1f**. In **1i**, the four hydrogen bonds possess an equal strength and are thus represented by a unique peak at -0.02 a.u. In the Möbius topology **1f**, the single hydrogen bond is stronger (ρ = -0.029 a.u.) than the hydrogen bonds in **1i**, whereas the bifurcated one is weaker (ρ = -0.014 a.u). Moreover, the figure-eight topology presents a delocalized π-π stacking at the central twist while a weaker and more localized CH-π interaction is observed in **1f**.

In order to analyse the dependence of the relative energies with the functional, the conformational analysis of unsubstituted [36]octaphyrin has been also performed with the B3LYP functional (Table S6). This functional was previously proven to predict geometries and thermochemistry of penta-,[20] hexa-[18] and heptaphyrins[21] in very good agreement with the experimental data. Remarkably, the correlation between the relative Gibbs free energies computed with both functionals is

Journal Name

ARTICLE

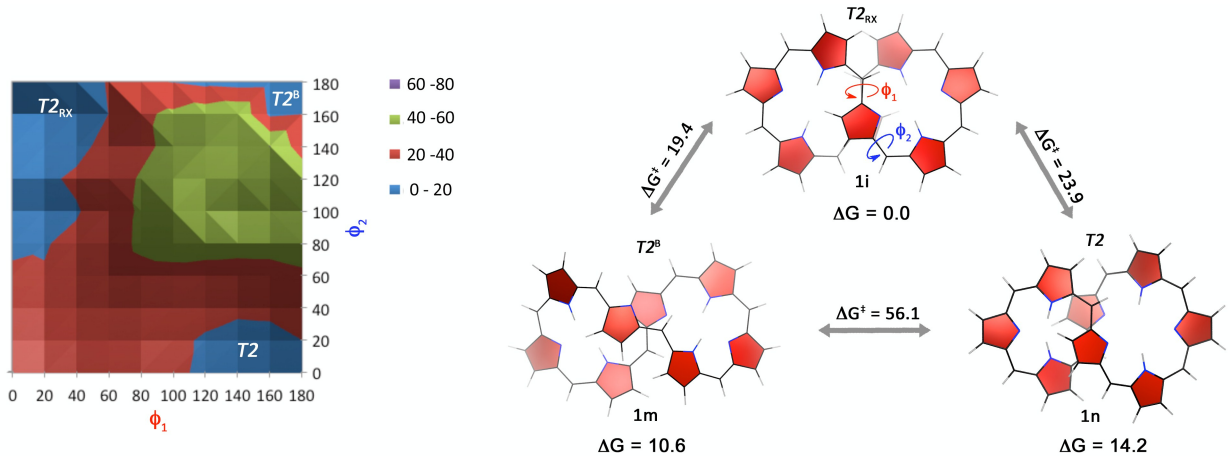

Fig. 5 M06/6-31G(d,p) relaxed potential energy surface for the figure-eight conformation (**1i**) obtained by rotating the dihedral angles ϕ_1 and ϕ_2 (in °). The fully optimized geometries for the different minima and the corresponding Gibbs free energies and activation energies are also shown.

high (R^2 = 0.89) and both methods predict that the figure-eight **1i** is the most stable (Fig. S5). The mean absolute difference between M06 and B3LYP is 5.3 kcal mol^{-1}. Generally, M06 predicts larger ΔG differences between the figure-eight and the Möbius and Hückel structures than B3LYP. So, the M06 functional might overestimate the stabilization of the twisted-Hückel topologies in octaphyrins, similarly to heptaphyrins.[21]

Interconversion pathways of neutral unsubstituted [36]octaphyrin

We have computed the activation energies for the interconversions between the most relevant conformations. In order to locate the transition states for the different interconversion pathways, we performed a series of 1D and 2D relaxed potential energy surfaces (PES) scans of **1** (Figs S11-S13). Similarly to other expanded porphyrins, the interconversion between different π-conjugation topologies is achieved by variation of internal dihedral angles.[18-21] The surface plot of the energy *versus* the dihedral angles ϕ_1 and ϕ_2 from the global minima **1i** is shown in Fig. 5. The low-energy pathway corresponds to the inversion of one pyrrole ring ($T2_{RX}$ ⟶ $T2^{B}$), leading to the conformation **1m**, which is 10.6 kcal mol^{-1} less stable than **1i**. The activation barrier for the **1i** ⟶**1m** interconversion is fairly large and a distorted Möbius topology was found as transition state. An alternative pathway involves the interconversion of **1i** into an asymmetric figure-eight conformation **1n** ($T2_{RX}$ ⟶ $T2$), in which the two hemicycles have not the same length. The activation barrier is even larger and a Möbius transition state was again located.

Additional calculations showed that the energy barriers for the switching between twisted-Hückel topologies are large (ΔG‡ ranges from 19.4 to 47.7 kcal mol^{-1}, Fig. S10). However, for the the interconversion process between figure-eight and Möbius conformers, the energy barrier is significantly lower, as shown in Fig. 6 for the $T2^{B,F}$ (**1g**) ⟶ $T1^{B,C,F}$ (**1f**) interconversion. Similarly, a low energy barrier is predicted for the Hückel-Möbius interconversion $T1^{B,C,E,H}$ (**1e**) ⟶ $T0^{B,C,E,G}$ (**1k**). These results point out that the figure-eight conformation **1i** is particularly stable in [36]octaphyrins and the presence of a number of intramolecular hydrogen bonds and π-π stacking hinder the interconversion between several twisted-Hückel topologies. Conversely, the switching between Möbius and Hückel conformers is feasible since the hydrogen bonding interactions are conserved along the interconversion pathways.

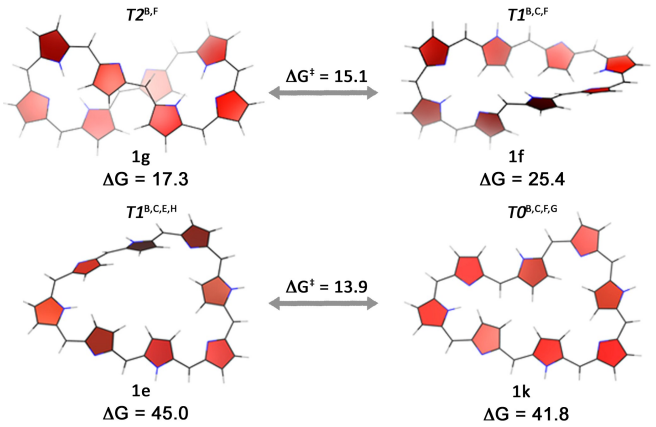

Fig. 6 Activation barriers (ΔG‡ in kcal mol^{-1}) for different topological interconversions in **1**. The Gibbs free energies with respect the global minimum **1a** are also shown.

Substituent effect on the conformation of neutral [36]octaphyrins

Since peripheral modifications at *meso*- and β-positions are very effective for tuning the conformational properties of expanded porphyrins,[20-21,51,52] we have investigated the effect of three substituents (CF_3, C_6F_5 and $C_6H_3Cl_2$) at the *meso* positions on the conformations of the neutral [36]octaphyrins. These substituents vary in steric effect and they are commonly used in the synthesis of expanded porphyrins.[27,10a] In this study, perfluorinated octaphyrins with fluorine substituents at both the *meso*-aryl and β-pyrrole positions were also considered since the X-ray structure of the [36]octaphyrin is markedly different from that of its β-hydrogen counterpart.[53] Table 2 collects the relative Gibbs free energy of the different neutral *meso*- and β-substituted [36]octaphyrins. Due to optimization issues, we could find neither an optimum geometry for $T2^{B,F}$ for aryl-substituted octaphyrins nor a minimum structure for $T0^{B,F,20,25}$.

In the neutral substituted [36]octaphyrins, the figure-eight structure **i** ($T2_{RX}$) is preferred over the other conformations. Our theoretical predictions are in good agreement with the experimental results available for *meso*-octakis(pentafluorophenyl) [36]octaphyrin since the X-ray diffraction analysis revealed a similar figure-eight structure.[27] Nevertheless, in the case of perfluorinated [36]octaphyrin, the crystallographic structure corresponds to the Hückel conformer **a** ($T0^{5,10,25,30}$),[53] in which the central pyrrole rings are largely tilted from the mean plane. However, our gas-phase Gibbs free energies point out that the $T2_{RX}$ is 19 kcal mol^{-1} more stable than the crystallographic structure $T0^{5,10,25,30}$ for the perfluorinated [36]octaphyrin. When solvation effects are taken into account, the ΔG difference is reduced to 14 kcal mol^{-1}.

Table 2. Relative Gibbs free energies (in kcal mol^{-1}) and hydrogen bonding index (N_H) of the different conformations of neutral meso- and β-substituted [36]octaphyrins.[a]

conf	Tn^X	-H	-CF_3	-C_6F_5	-$C_6H_3Cl_2$	-C_6F_5,-F	-OMe
a	$T0^{5,10,25,30}$	20.0	6.7	16.8	16.6	19.2	0.0
b	$T0^{B,C,E,F,H}$	41.3	41.2	41.4	38.3	44.2	38.4
c	$T0^{B,F,5,20,25}$	25.5	5.2	18.3	8.3	14.2	15.0
e	$T1^{B,C,E,H}$	45.0	30.1	40.6	31.7	42.4	37.8
f	$T1^{B,C,F}$	25.4	14.8	10.1	7.4	15.7	13.5
g	$T2^{B,F}$	17.3	10.1	-	-	-	3.8
h	$T2^{C,G}$	15.5	3.9	5.4	4.0	11.6	2.5
i	$T2_{RX}$	0.0	0.0	0.0	0.0	0.0	0.0

[a] Gibbs free energies at the M06/6-311+G(d,p)//M06/6-31G(d,p) level of theory.

The incorporation of *meso*-substituents leads to a stabilization of the Hückel and Möbius conformers and the magnitude of such stabilization depends on the nature of the substituents (Fig. S16). For instance, the ΔG difference between $T0^{B,F,5,20,25}$ and the $T2_{RX}$ structures is reduced to 5 and 8 kcal mol^{-1} with the bulky CF_3 and $C_6H_3Cl_2$ groups, respectively, whereas it is 18 kcal mol^{-1} for the C_6F_5 groups. For the trifluoromethyl group, the Hückel untwisted conformers **a** and **c** are relatively stable with energy differences with respect to $T2_{RX}$ of 3 and 6 kcal mol^{-1}. Furthermore, an alternative figure-eight conformation with two inverted pyrrole rings **h** is also viable for the CF_3 group. This substituent increases the ring strain (Φ_p = 29.3) and reduces importantly the π-conjugation in the doubly-twisted topology **i** (Π = 0.46, Table S10). In this case, the ring strain of the $T2_{RX}$ is reduced by inversion of two pyrrole rings ($T2^{C,G}$: Φ_p = 21.3 and Π = 0.53). Thus, the *meso*-trifluoromethyl octaphyrin could exist in solution as equilibrium of several figure-eight and Hückel conformers.

In the case of the C_6F_5 and $C_6H_3Cl_2$ substituents, neutral [36]octaphyrins prefer the conformation $T2_{RX}$ because this structure combines the lowest macrocyclic strain and the highest number of intramolecular hydrogen bonding (Table S11). It is noteworthy that the changes in ring strain and overall π-conjugation imposed by the aryl groups are less pronounced than with the CF_3 groups, allowing an effective π-conjugation in the figure eight-topology (Φ_p = 21.6 and Π = 0.65). Interestingly, the Möbius conformer $T1^{B,C,F}$ is further stabilized with the $C_6H_3Cl_2$ group, which reduces its relative ΔG to 7.4 kcal mol^{-1}. Hence, although neutral substituted [36]octaphyrins prefer a figure-eight conformation, the relative stability of the Hückel and Möbius conformers can be fine-tuned by the *meso*-and β-substituents.

Although electron-withdrawing groups are required for the formation of expanded porphyrins using the Rothemund-Lindsey protocol,[27] we have also investigated how the presence of electron-donating groups (OMe) at *meso* positions modify the conformational preferences of neutral [36]octaphyrin. In the presence of the OMe susbtituent, the twisted-Hückel conformer **i** ($T2_{RX}$) and the untwisted Hückel conformer **a** ($T0^{5,10,25,30}$) become almost isoenergetic. With this substituent, the Hückel structure becomes highly stabilized due to the presence of additional NH···O hydrogen bonds (Fig. S17). Still, the Möbius topologies are high in energy, indicating that a singly-twisted topology is not likely for neutral [36]octaphyrins regardless of the electronic nature of the substituent.

Conformational changes upon protonation and redox reactions

As redox reactions and protonation were found to induce conformational changes in several expanded porphyrins,[23,25] we have investigated them as potential chemical triggers to induce conformational and/or aromaticity switches in octaphyrins. Experimentally, it was proven that the change of the oxidation state in [36]octaphyrin is coupled to large changes in the absorption spectra that were explained in terms of a switch from antiaromatic twisted-Hückel to aromatic Hückel species.[27] Nevertheless, the structures of the oxidized and reduced forms corresponding to [34] and [38] π-electrons are still unknown. Alternatively, protonation can be used for controlling the molecular topology of [36]octaphyrin, as shown recently by Osuka *et al*.[28] Eventually, the combination of protonation and reduction of the macrocycle

has also been investigated by analysing the behaviour of [38]octaphyrins upon protonation.

The relative Gibbs free energies of neutral and diprotonated octaphyrins with varying oxidation states are collected in Table 3. Except for neutral [34]octaphyrin **2** and diprotonated [36]octaphyrin **4**, the figure-eight conformation $T2_{RX}$ is still the global minimum in all the unsubstituted octaphyrins in gas-phase calculations. For **2** and **4**, an alternative twisted-Hückel structure with two inverted pyrrole rings is preferred. Nevertheless, the variation of oxidation state and especially protonation decrease the conformational preference of octaphyrins for the figure-eight conformation, reducing the relative energy of Hückel and Möbius conformers (Table 3).

With [34] π-electrons, the stability of untwisted Hückel topologies is significantly enhanced compared to [36]octaphyrin **1**. Considering the small energy differences between the *T2* and *T0* conformations, we anticipate that [34]octaphyrins could exist in solution as an equilibrium of Hückel and twisted-Hückel structures. The higher stability of the Hückel conformers is related to their lower ring strain, effective hydrogen bonding and the presence of aromaticity (Table S12). The Möbius conformations **2e** and **2f** are 40 and 17 kcal mol^{-1} higher in energy, so singly-twisted topologies are very unlikely for **2**.

Table 3. Relative Gibbs free energies (in kcal mol^{-1}) of the different conformations of neutral and diprotonated unsubstituted octaphyrins with different oxidation states.[a]

conf	Tn^{X}	[36] (**1**)	[34] (**2**)	[38] (**3**)	$[36]^{2+}$ (**4**)	$[38]^{2+}$ (**5**)
a	$T0^{5,10,25,30}$	20.0	4.1	14.8	4.3	10.2
b	$T0^{B,C,E,F,H}$	41.3	33.3	48.8	34.7	4.9
c	$T0^{B,F,5,20,25}$	25.5	9.7	16.5	9.7	10.5
d	$T0^{B,F,20,25}$	31.4	14.4	20.4	14.8	13.7
e	$T1^{B,C,E,H}$	45.0	39.6	51.9	29.7	13.0
f	$T1^{B,C,F}$	25.4	16.6	25.7	2.7	9.2
g	$T2^{B,F}$	17.3	0.0	7.9	0.3	2.2
h	$T2^{C,G}$	15.5	0.0	6.8	0.0	4.6
i	$T2_{RX}$	0.0	6.5	0.0	3.4	0.0
	MAD[b]	-	*12.2*	*6.4*	*14.3*	*17.0*

[a] Gibbs free energies at the M06/6-311+G(d,p)//M06/6-31G(d,p) level of theory. [b] *MAD* is the mean absolute difference with respect the relative Gibbs free energies of unsubstituted [36]octaphyrin **1**.

By contrast, [38]octaphyrin **3** can only adopt figure-eight topologies **3g**-**i** since the Gibbs free energies of the Hückel and Möbius topologies exceed 15 kcal mol^{-1}. In general, the reduction of [36]octaphyrin affects in a lesser extent the conformational relative Gibbs free energies compared to the oxidation of the macrocycle. With [38] π-electrons, the Möbius structures are highly destabilized, being 52 and 26 kcal mol^{-1} higher in energy than the figure-eight conformation **3i**. This structure is still preferred over the other conformations due to its low ring strain and effective overlap of the *p* orbitals (Table S13). Therefore, the variation of the oxidation state is not an effective *stimulus* to produce Möbius species in octaphyrins, although it leads to aromaticity switches transforming non-aromatic twisted-Hückel topologies ([4*n*] π-electrons) into aromatic ones ([4*n* + 2] π-electrons) (see below).

The conformational stability of both [34] and [38]octaphyrins is still governed by the number of hydrogen bonds, although in a lesser extent than in [36]octaphyrins. The NCI and geometrical analysis indicate that there is a weakening of the hydrogen bonds and the π–π stacking interaction in the figure-eight topology upon oxidation (Figs. S21-22). By contrast, the intramolecular hydrogen bonds and the π–π stacking interactions are strengthened upon reduction, as can be inferred from the shortest NH···N lengths and the reduced distance between the stacked pyrrole rings in the figure-eight conformation with [38] π-electrons. These results suggest that the conformational preference of octaphyrins for twisted-Hückel topologies diminishes with the weakening of hydrogen bonds and the π-π stacking interaction.

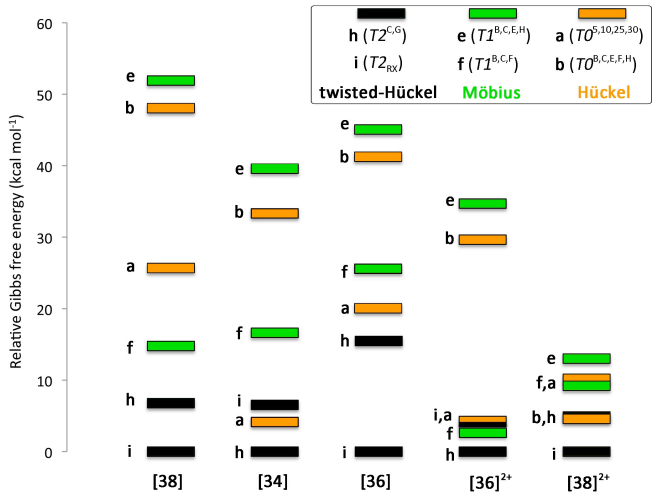

Fig. 7 Relative Gibbs free energies computed for the different structures of unsubstituted octaphyrins with different oxidation and protonation state.

Protonation seems to be more effective than redox reactions for triggering a conformational switch in unsubstituted [36]octaphyrin (Fig. 7). Beside the figure-eight conformations, diprotonated [36]octaphyrin **4** could easily adopt a Möbius conformer (**4f**), whose relative Gibbs free energies do not exceed 3 kcal mol^{-1}. Importantly, the Möbius structures **4e** and **4f** are stabilized by 15 and 23 kcal mol^{-1} in the diprotonated state towards their neutral counterparts. However, the figure-eight topology **4h** still remains the global minimum in diprotonated [36]octaphyrin mainly due to its lower ring strain and more effective π network (Table S14).

The situation is different in diprotonated [38]octaphyrin **5** where the untwisted Hückel conformers (**5a-c**) are more stable than the singly-twisted conformations (**5e**-**f**). Interestingly, the Hückel conformation with five inverted pyrrole rings (**5b**) is highly stabilized in diprotonated [38]octaphyrins. It is noteworthy that a similar structure was revealed by the X-ray

diffraction analysis of diprotonated *meso*-octakis(pentafluorophenyl) [38]octaphyrin.[28] Owing to the lack of intramolecular hydrogen bonds in **5**, the conformational predominance of twisted-Hückel conformers is largely reduced in this case. The importance of the ring strain in the conformational stabilities of **5** is larger and there is a rough correlation between the relative energies and Φ_p (R^2 = 0.61, Fig. S23). Nevertheless, our calculations indicates that the figure-eight topology **5i** corresponds to the global minimum for unsubstituted [38]octaphyrins in the diprotonated state because of its low ring strain and the most effective π-conjugation (Table S15).

Conformational changes of *meso*-octakis(pentafluorophenyl) octaphyrins upon protonation and redox reactions

In the next step, we have investigated the stability of *meso*-octakis(pentafluorophenyl) octaphyrins with different oxidation and protonation states in both gas-phase and solvent. Experimental information about these *meso*-aryl substituted octaphyrins is currently available,[27,28] being certainly appropriate to test our computational results. The relative Gibbs free energies computed for the *meso*-octakis(pentafluorophenyl) [36] and [38]octaphyrins in neutral and diprotonated states are collected in Table 4.

In general, the inclusion of solvent reduces significantly the relative Gibbs free energies of those conformers having more inverted pyrrole rings, such as **b** and **e**. In both cases, the inverted pyrrole rings might be involved in intermolecular hydrogen bonds with the solvent molecules, thus reducing their respective relative ΔG by more than 16 kcal mol^{-1} in the neutral state.

According to the relative ΔG computed with M06, the figure-eight conformations are viable for *meso*-octakis(pentafluorophenyl) [36] and [38]octaphyrins in both neutral and diprotonated states. For the neutral [36]octaphyrin **6**, the global minima corresponds to the twisted-Hückel topology **6i** with all the pyrrolic nitrogens pointing inward, in good agreement with the X-ray crystallographic structure.[27] Similarly to unsubstituted [36]octaphyrin, the conformation **6i** is preferred over the Möbius and Hückel structures because of its effective intramolecular hydrogen bonds and lower ring strain. Consequently, the overlap of *p*-orbitals is more effective in the doubly-twisted topology (Table S16). An alternative figure-eight conformation **6h** with two inverted pyrrole rings is also viable in solution. Nevertheless, the computed ^{1}H NMR spectrum of the conformation **6i** resembles the experimental spectrum of neutral [36]octaphyrin in a larger extent than that of the conformer **6h** (Fig. S29). In the experimental ^{1}H NMR spectrum, the β-protons appear at 6-8 ppm region whereas the NH protons resonate at 13.3 and 8.6 ppm, indicating a non-aromatic structure.[27] However, the NH protons of the conformer **6h** are largely deshielded (17 and 20 ppm) and the β-protons of the inverted pyrrole rings appear at 5-8 ppm. These signals disappear in the conformer **6i** and the computed ^{1}H chemical shifts are in better agreement with the experimental ones (Fig. S29). Therefore, our calculations point out that *meso*-octakis(pentafluorophenyl) [36]octaphyrin adopts preferentially the figure-eight conformation **6i** in the solid-state and in solution.

Table 4. Relative Gibbs free energies (in kcal mol^{-1}) of the different conformations of neutral and diprotonated *meso*-octakis(pentafluorophenyl) [36] and [38]octaphyrins.[a]

conf	Tn^X	[36] (**6**)	[38] (**7**)	$[36]^{2+}$ (**8**)	$[38]^{2+}$ (**9**)
a	$T0^{5,10,25,30}$	16.8 (14.4)	16.7 (17.9)	4.9 (8.6)	6.1 (8.2)
b	$T0^{B,C,E,F,H}$	41.4 (23.4)	39.4 (24.6)	32.6 (23.6)	1.3 (2.4)[c]
c	$T0^{B,F,5,20,25}$	18.3 (16.2)	7.3 (8.7)	8.1 (13.6)	6.5 (12.1)
d	$T0^{B,F,20,25}$	25.4 (23.2)	19.5 (21.4)	21.5 (23.6)	15.6 (20.3)
e	$T1^{B,C,E,H}$	40.6 (24.1)	44.1 (31.2)	29.0 (23.1)[c]	7.0 (5.6)
f	$T1^{B,C,F}$	10.1 (1.8)	12.3 (8.0)	5.0 (2.1)	3.5 (5.7)
h	$T2^{C,G}$	5.4 (1.7)	0.0 (0.0)	0.0 (0.0)	0.0 (0.0)
i	*T2*	0.0 (0.0)[c]	7.5 (8.6)	15.8 (11.1)	5.9 (3.0)
	MAD[b]	-	*4.7 (4.7)*	*9.1 (2.9)*	*12.6 (7.7)*

[a] Gibbs free energies at the M06/6-311+G(d,p)//M06/6-31G(d,p) level of theory in gas-phase and solvent (in parenthesis). [b] *MAD* is the mean absolute difference with respect the relative Gibbs free energies of neutral [36]octaphyrin **6.** [c] The X-ray structure corresponds to this conformation.

For the *meso*-substituted [38]octaphyrin (**7**), the relative Gibbs free energies indicate that the figure-eight conformation **7h** with two inverted pyrrole rings is the most stable. In this case, a Hückel conformation **7c** ($T0^{B,F,5,20,25}$) is highly stabilized upon reduction of the macrocycle. This Hückel structure is highly non-planar and non-symmetric with two sets of three pyrrole rings in a relatively planar arrangement and the central inverted pyrrole rings largely tilted from such planes. Interestingly, a similar structure was observed in the solid state of the *meso*-β-perfluorinated [38]octaphyrin.[53] Although no crystallographic structure is available for **7**, a related Hückel conformation $T0^{B,F,20,25}$ (**d**) was proposed by Osuka *et al* on the basis of the ^{1}H NMR spectroscopy.[28] However, the conformer **7d** is not viable according to our computed Gibbs free energies in gas-phase and solvent. The careful inspection of the optimized geometries of the figure-eight conformer **7h** and the Hückel conformers **7c** and **7d** reveals that four intramolecular hydrogen bonds (N_H = 3) stabilized all the structures, although the shorter NH···N distances are found in **7c** and **7h** (Fig. S28). The torsional ring strain is significantly reduced in the twisted-Hückel topology, leading to a more effective π-conjugation than in the Hückel topologies. Consequently, the twisted-Hückel conformation **h** is predicted to be the most stable for **7**. In order to confirm our computational predictions, the ^{1}H-NMR spectra of the three plausible conformations have been computed at the B3LYP/6-311+G(d,p) level of theory in chloroform. The calculated and experimental values of the ^{1}H NMR chemical shifts are displayed in Fig. 8. It is noteworthy that the experimental ^{1}H NMR spectrum of **7** indicates the

presence of a moderate diatropic ring current by showing β-proton signals in two separated regions: 5.5-7.0 ppm for the outer β-protons and 2.5-3.0 ppm for the inner β-protons attached to the inverted pyrrole rings.[28]

The discrepancy between the computed and experimental ^{1}H NMR spectra for the Hückel conformers **7c** and **7d** supports the idea that these Hückel conformers are not the predominant conformations for the [38]octaphyrin. On one side, the NH protons of the inverted pyrrole rings and the outer pyrrolic β-protons of **7d** are markedly deshielded compared to the experimental values. On the other side, the computed ^{1}H-NMR spectrum of **7c** reveals the presence of a large number of signals for both the NH protons and the β-protons, as a consequence of the non-symmetric structure. In addition, several NH signals in **c** appear between 3-5.5 ppm and no signals appear in this region in the experimental spectrum. On the contrary, the computed ^{1}H NMR spectrum of **7h** resembles the experimental one. The β-protons signals appear at two different regions around 2 ppm and 6 ppm, respectively. Therefore, on the basis of our calculations, the most plausible structure for the neutral *meso*-octakis(pentafluorophenyl) [38]octaphyrin is the figure-eight conformation **7h** with two inverted pyrrole rings. This conformation with [38] π-electrons is expected to be moderately aromatic according to the Hückel´s rule.

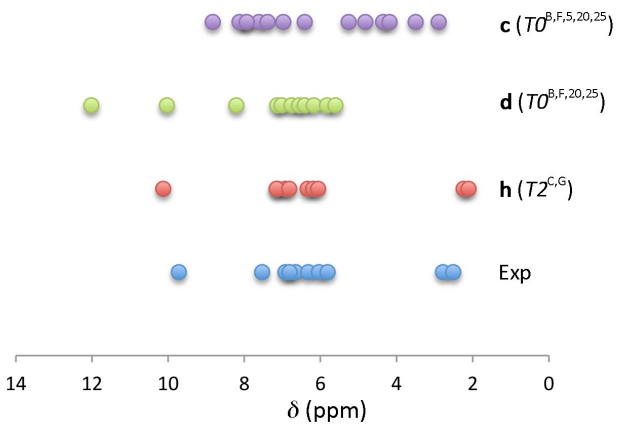

Fig. 8 Experimental and computed ^{1}H NMR shifts of the NH protons and β-protons for the neutral [38]octaphyrin **7** in different conformations.

Protonation induces a larger change in the ΔG of *meso*-subtituted [36]octaphyrin, as can be inferred from Table 4. In the diprotonated state, the most stable conformations correspond to a figure-eight conformation **h** and a Möbius topology **f**, which is only 2.1 kcal mol^{-1} higher in energy in trifluoroacetic acid. However, the X-ray diffraction analysis revealed a Möbius structure with four inverted pyrrole rings, similar to conformation **e**, which is involved in an extensive network of intermolecular hydrogen bonds with TFA molecules and their counter-anions.[28] According to our calculations, this conformation is 23.1 kcal mol^{-1} higher in energy than the global minimum. The discrepancy between the experimental and computational results can be related to the lack of counter-anions in our structures and/or the overestimation of the stability of the diprotonated figure-eight topologies by M06. In a previous work, we found that M06-2X and B3LYP-D failed in describing correctly the stability of the Möbius conformer upon protonation in the [32]heptaphyrin. Only B3LYP predicted the Möbius topology as most stable in agreement with the solid-state structure.[21]

To discard the second possibility, we have performed single-point calculations to evaluate the relative ΔGs at the B3LYP/6-311+G(d,p)//M06/6-31G(d,p). The B3LYP-recomputed ΔG_{solv} (in kcal mol^{-1}) are 0.0 (**8f**), 6.1 (**8e**), 12.2 (**8b**) and 14.1 (**8h**) (Table S20). So, importantly, the B3LYP energies indicate that the Möbius structures are by far the most stable conformations in diprotonated [36]octaphyrin, in better agreement with the experimental observations.[28] In fact, the computed ^{1}H NMR spectra of the Möbius conformers **8e** and **8f** are in better agreement with the experimental spectra than that of the figure-eight topology **8i** (Fig. S30). Both Möbius structures present signals in the region 0 and -6 ppm, which indicates a substantial diatropic ring current. However, as the figure-eight conformation **8i** only possess inward pointing NH groups and out outward pointing β–protons, all its protons are significantly deshielded with respect to the experimental data. Therefore, a Möbius conformation is preferred for diprotonated *meso*-C_6F_5 [36]octaphyrin **8**.

For diprotonated *meso*-C_6F_5 [38]octaphyrin **9**, the relative ΔGs point out that figure-eight conformers (**9h-i**), Möbius topologies (**9e-f**) and a Hückel conformations (**9b**) are viable considering the small energy differences among these conformations. Although the most stable conformer is again the figure-eight conformation **9h**, the Hückel conformer **9b** is greatly stabilized in **9**, being just 1.3 kcal mol^{-1} higher in energy than **9h**. Importantly, the crystallographic structure of **9** corresponds to the Hückel conformation **9b**, where the octaphyrin macrocycle is surrounded by TFA molecules to form an extensive intermolecular hydrogen bond network.[28] At the B3LYP level, the conformation **9b** is indeed the global minima, followed by the Möbius **9e** (ΔG = 6.8 kcal mol^{-1}) (Table S20). Again, the twisted-Hückel topologies raised in energy relative to the ΔGs computed with M06. For instance, the relative ΔG of **9h** increases from 0.0 to 20.2 kcal mol^{-1} as the functional changes from M06 to B3LYP.

Although topologically different, the Hückel **9b** and Möbius **9e** structures are similar except from the dihedral angles in the tilted pyrrole ring. In the case of diprotonated [38]octaphyrin, the Hückel **9b** is more stable than the Möbius **9e** mainly due to the expected aromatic stabilization in the Hückel [4*n* +2] π-electron system. On the contrary, the Möbius conformation **8e** is more stable than the Hückel one **8b** in the diprotonated [36]octaphyrin owing to the Möbius aromatic stabilization in [4*n*] π-electron system. Thus, aromaticity seems to control the molecular topology of diprotonated octaphyrins, as previously observed experimentally by Osuka *et al.*[28]

Therefore, protonation is an effective method to induce topological switches in octaphyrins. Whereas diprotonated [36]octaphyrin adopts a Möbius structure, diprotonated [38]octaphyrin prefers a Hückel untwisted conformation. By contrast, the figure-eight topology is kept after oxidation or

reduction of the macrocycle, although two pyrrole rings are inverted upon reduction.

Structure-aromaticity relationship in Hückel and Möbius octaphyrins

Although the multidimensional character of aromaticity has been recognized for a decade,[16] most of the experimental studies on expanded porphyrins solely employed NICS as an aromatic index. Recent computational studies demonstrated that several indices of aromaticity should be used to quantify the aromaticity of expanded porphyrins accurately.[17,18,20-21,54] Although the different indices are correlated, these correlations depend on the data set. Moreover, we previously found that the aromaticity of expanded porphyrins is revealed best by the magnetic indices and the relative hardness rather than the structural and energetic descriptors.[18,20] Our structure-property relationships demonstrated that the aromaticity of expanded porphyrins is highly dependent on the molecular topology and the number of π-electrons. Here, we investigate the aromaticity of octaphyrins exhibiting different molecular topologies and different number of π-electrons using energetic, magnetic, structural and reactivity criteria. Additionally, the performance of the different indices to describe Hückel and Möbius aromaticity in octaphyrins is also analysed.

The different indices of neutral [36]octaphyrin **1** were computed using the M06 and B3LYP functionals and, in general, good correlations were found between the aromaticity descriptors computed with the two density functionals (Figs. S31-S32). However, M06-computed NICS values are usually shifted to the antiaromatic region providing smaller absolute NICS-indices for aromatic conformations and higher NICS-indices for antiaromatic ones. As the B3LYP functional was used previously to evaluate the aromaticity descriptors of penta-, hexa- and heptaphyrins,[18,20-21] we decided to focus on the B3LYP-computed indices. Moreover, B3LYP provides aromaticity indices that are more strongly correlated to each other than M06.

First, we investigated the aromaticity of the different conformations of the neutral unsubstituted [36]octaphyrin **1** in order to determine the relationship between the molecular conformation and macrocyclic aromaticity. Table 5 collects the energetic (ISE), magnetic [Λ, NICS(0) and $NICS_{zz}(1)$], structural (HOMA) and reactivity ($\Delta\eta$) indices computed with the B3LYP functional for the Hückel, Möbius and twisted-Hückel conformations of **1**.

Table 5 illustrates that there is a close relationship between molecular topology (Hückel, Möbius and twisted-Hückel) and aromaticity in [36]octaphyrins. On the one hand, Möbius topologies (**1e**-**f**) are clearly aromatic with positive ISE_{corr} and $\Delta\eta$ values and exhibit strong diatropic ring currents. In addition, the degree of bond-equalization is enhanced in Möbius topologies, as shown by the HOMA index. On the other hand, Hückel topologies with [36] π-electrons (**1a**-**d**) display highly positive values of NICS-based indices and Λ, coupled to negative ISE_{corr} and $\Delta\eta$, which denotes antiaromaticity. Interestingly, the strength of the induced ring current is related to the ring strain and the efficiency of π-conjugation. Hence, the strongest paramagnetic ring current is found in **1a** (Φ_P = 13.0 and Π = 0.83, Table S7).

Table 5. Energetic, reactivity, magnetic and structural indices of aromaticity of the different conformations of the neutral unsubstituted [36]octaphyrin **1**.[a]

conf	Tn^X	ISE	ISE_{corr}	$\Delta\eta$	Λ	NICS(0)	$NICS_{zz}(1)$	HOMA
1a	$T0^{5,10,25,30}$	26.6	2.4[b]	-3.0	422	16.8	51.2	0.73
1b	$T0^{B,C,E,F,H}$	18.7	-2.4	-6.2	707	12.3	38.3	0.71
1c	$T0^{B,F,5,20,25}$	12.8	-3.0	-3.0	462	-0.2	37.9	0.73
1d	$T0^{B,F,20,25}$	23.1	-2.4	-3.6	268	5.0	24.4	0.73
1e	$T1^{B,C,E,H}$	22.3	7.9	3.9	-488	-9.3	-22.6	0.79
1f	$T1^{B,C,F}$	24.1	2.7	3.8	-344	-15.6	-32.0	0.85
1g	$T2^{B,F}$	23.3	-0.1	-5.4	193	8.5	-20.2	0.74
1h	$T2^{C,G}$	23.2	1.6[b]	-6.7	150	10.2	-17.2	0.72
1i	$T2_{RX}$	20.5	2.1[b]	-3.8	22	-2.6	-19.5	0.75

[a] ISE, ISE_{corr} and $\Delta\eta$ are given in kcal mol^{-1}, Λ in ppm cgs and NICS indices in ppm. [b] The large flexibility induces topology changes in the dihydrogen derivative of the methylene adducts during the optimization.

The twisted-Hückel topologies **1g**-**i** have small ISE_{corr} values, negative $\Delta\eta$ and positive Λ, whose magnitude is strongly reduced towards untwisted conformations. The reduced values of the magnetic indices imply that the induced paramagnetic ring current is considerably smaller in the figure-eight conformations, especially in the global minimum **1i**.[55] In fact, the NICS(0) and Λ supports a non-aromatic character for **1i,** in agreement with the ^{1}H NMR spectra of the neutral [36]octaphyrin.[27] Importantly, the $NICS_{zz}(1)$ values of the figure-eight conformations are negative indicating aromatic character. In these doubly twisted conformations, the "probe atom" at 1 Å above the mean molecular plane is located near the stacked pyrrole rings, reflecting the local diatropic ring current of the individual pyrrole rings. So, $NICS_{zz}(1)$ is not adequate to evaluate the macrocyclic aromaticity in the twisted-Hückel conformations. The spurious contributions of the currents of adjacent rings on the NICS indices have been previously reported in other π-conjugated systems.[16a,56]

From the energetic point of view, the effect of the aromatic stabilization/destabilization in octaphyrins is much weaker than in small monocycles like benzene (ISE_{corr} = 34.3 kcal mol^{-1}). This explains why antiaromatic [36]octaphyrins are also viable. In these large macrocycles, the aromatic destabilization is not strong enough to compensate the most effective hydrogen bonding in the twisted-Hückel topology. For this reason, aromaticity plays a minor role in the determination of the relative stability of the conformations of neutral [36]octaphyrins, although the photophysical and nonlinear optical properties of octaphyrins are highly dependent on the macrocyclic aromaticity.[12,13]

In the annulene model, the aromaticity of octaphyrins can be predicted according to the number of π-electrons within the

annulene-type conjugation pathway.[34] Consequently, the aromaticity of octaphyrins is expected to be reversed upon redox reactions, which modify the number of π-electrons within the classical conjugation pathway. In order to verify this assumption, the degree of aromaticity of neutral unsubstituted [34] and [38]octaphyrins (**2** and **3**) was quantified with structural (HOMA), magnetic (NICS, Λ), reactivity ($\Delta\eta$) and energy criteria (ISE_{corr}) (Table 6).

Table 6. Energetic, reactivity, magnetic and structural indices of aromaticity of the different conformations of the neutral unsubstituted [34]- and [38]octaphyrins **2** and **3**.[a]

conf	Tn^X	ISE	ISE_{corr}	$\Delta\eta$	Λ	NICS(0)	$NICS_{zz}(1)$	HOMA
2a	$T0^{5,10,25,30}$	27.4	-2.8[b]	4.1	-445	-15.2	-34.2	0.81
2c	$T0^{B,F,5,20,25}$	23.4	-2.0[b]	0.5	-192	-21.6	-29.1	0.82
2e	$T1^{B,C,E,H}$	17.4	-0.4	-5.1	349	5.4	19.6	0.71
2f	$T1^{B,C,F}$	15.1	-4.6	-6.2	347	10.8	33.5	0.78
2h	$T2^{C,G}$	25.7	-12.6[b]	3.6	-127	-12.7	-20.9	0.84
2i	$T2_{RX}$	23.8	11.7	-1.2	-30	-3.2	-9.3	0.85
3a	$T0^{5,10,25,30}$	29.3	-13.5[b]	1.1	-492	-18.2	-37.3	0.84
3c	$T0^{B,F,5,20,25}$	33.9	-9.8[b]	9.1	-159	-8.6	-9.0	0.82
3e	$T1^{B,C,E,H}$	28.5	-9.4	4.9	307	5.0	18.3	0.73
3f	$T1^{B,C,F}$	20.8	-6.2	-3.4	325	10.4	34.5	0.83
3h	$T2^{C,G}$	31.9	-12.1[b]	4.9	-158	-15.8	-41.2	0.87
3i	$T2_{RX}$	27.9	-9.0[b]	7.9	-107	-14.5	-44.1	0.88

[a] ISE, ISE_{corr} and $\Delta\eta$ are given in kcal mol^{-1}, Λ in ppm cgs and NICS indices in ppm. [b] The large flexibility induces topology changes in the dihydrogen derivative of the methylene adducts of these conformations during the optimization.

Consistent with the annulene model, the aromaticity of the twisted-Hückel, Hückel and Möbius topologies is totally reversed upon oxidation/reduction of the macrocycle. Consequently, Möbius conformations with [34] and [38] π-electrons are antiaromatic, as can be seen by the reversed sign of the aromatic descriptors with respect to the Möbius conformation of [36]octaphyrin (Fig. S33). The conformers **2f** and **3f** display strong paramagnetic ring currents whereas negative NICS and Λ are found for the counterpart **1f**. Moreover, the antiaromatic character of **2f** and **3f** is supported by their negative relative hardness. By contrast, the Hückel and figure-eight conformations become clearly aromatic upon two-electron redox reactions. In [4*n*+2] π-electron octaphyrins, Hückel conformations exhibit a strong diatropic current and positive $\Delta\eta$, which are indicative of aromatic systems. In addition, the HOMA index becomes lower in the Möbius topologies than in the Hückel and twisted-Hückel conformations of [34] and [38]octaphyrins. Even though Hückel conformers are aromatic in [34] and [38]octaphyrins, the variation of oxidation state gives rise to different values of the aromaticity descriptors for equivalent conformations. For instance, the figure-eight conformation **3i** is more aromatic than its homologous **2i**, according to the Λ, NICS(0), $\Delta\eta$ and HOMA.

Finally, the aromaticity of diprotonated unsubstituted [36] and [38]octaphyrins **4** and **5** has been evaluated using the same indices (Table 7). In contrast to redox reactions, protonation does not reverse the sign of the aromaticity descriptors of the conformations with respect to the neutral state. This is expected since the number of π-electrons along the conjugation pathway is the same for neutral and diprotonated species. Nevertheless, the strength of the induced ring current is enhanced in diprotonated conformers towards their neutral homologous. For instance, the aromaticity of the Möbius [36] π-electron conformations **e**-**f** significantly increases upon protonation, as shown by the larger $\Delta\eta$ and more negative magnetic descriptors for the diprotonated **4e**-**f**. Similarly, the aromaticity of the Hückel conformations **a**-**c** with [38] π-electrons is enhanced when going from the neutral to the diprotonated state. Therefore, diprotonated [38]octaphyrins combine the enhancement of the aromaticity indices upon protonation with the aromatic character of the Hückel topologies.

Table 7. Energetic, reactivity, magnetic and structural indices of aromaticity of the different conformations of the diprotonated unsubstituted [36]- and [38]octaphyrins **4** and **5**.[a]

conf	Tn^X	ISE	ISE_{corr}	$\Delta\eta$	Λ	NICS(0)	$NICS_{zz}(1)$	HOMA
4a	$T0^{5,10,25,30}$	22.1	-13.5	-7.3	881	28.4	81.7	0.69
4c	$T0^{B,F,5,20,25}$	16.1	-15.5	-9.2	479	5.1	37.1	0.80
4e	$T1^{B,C,E,H}$	26.2	0.95	10.8	-559	-10.4	-26.0	0.80
4f	$T1^{B,C,F}$	20.7	3.2	5.1	-361	-15.3	-30.9	0.71
4h	$T2^{C,G}$	20.9	-1.5	-8.0	379	18.6	-17.1	0.78
4i	$T2_{RX}$	25.1	0.3[b]	-3.4	70	1.2	-25.6	0.77
5a	$T0^{5,10,25,30}$	27.7	-13.0[b]	7.7	-638	-17.8	-39.2	0.88
5c	$T0^{A,E,5,25,40}$	22.1	-9.6[b]	6.7	-278	-18.5	-28.0	0.86
5e	$T0^{B,F,5,20,25}$	29.3	-14.2	-2.6	707	12.8	40.5	0.76
5f	$T1^{B,C,E,H}$	15.3	-15.6	-2.7	462	20.8	59.2	0.76
5h	$T1^{B,C,F}$	27.8	-2.4[b]	8.3	-283	-18.0	-21.1	0.87
5i	$T2_{RX}$	27.6	-13.0[b]	10.3	-183	-14.4	-33.5	0.88

[a] ISE, ISE_{corr} and $\Delta\eta$ are given in kcal mol^{-1}, Λ in ppm cgs and NICS indices in ppm. [b] The large flexibility induces topology changes in the dihydrogen derivative of the methylene adducts during the optimization.

The statistical analysis revealed significant correlations among the magnetic and reactivity descriptors of aromaticity, so NICS, Λ and $\Delta\eta$ distinguish between aromatic and antiaromatic octaphyrins in a roughly similar way (Table S26, Fig. 9). Interestingly, the isomerization method provides Λ and $\Delta\eta$ vales highly correlated with the NICS-based indices. By contrast, the energetic parameter ISE_{corr} is not correlated with the rest of indices. For the evaluation of the energetic descriptor, the application of *syn-anti* corrections is mandatory due to the *cis-trans* diene mismatches in the methyl and

methylene isomer.[19] The *syn-anti* corrections are evaluated as the energy difference between the dihydrogen derivative of the *meso*-methyl octaphyrin and its respective nonaromatic isomer (Scheme S1). However, most of the dihydrogen derivatives of the methylene isomers switch its topology during the optimization step, resulting in biased ISE_{corr} values. By contrast, the evaluation of the Λ and $\Delta\eta$ does no require *syn/anti* corrections, so the isomerization method is an effective approach for evaluating Λ and relative hardness of octaphyrins.

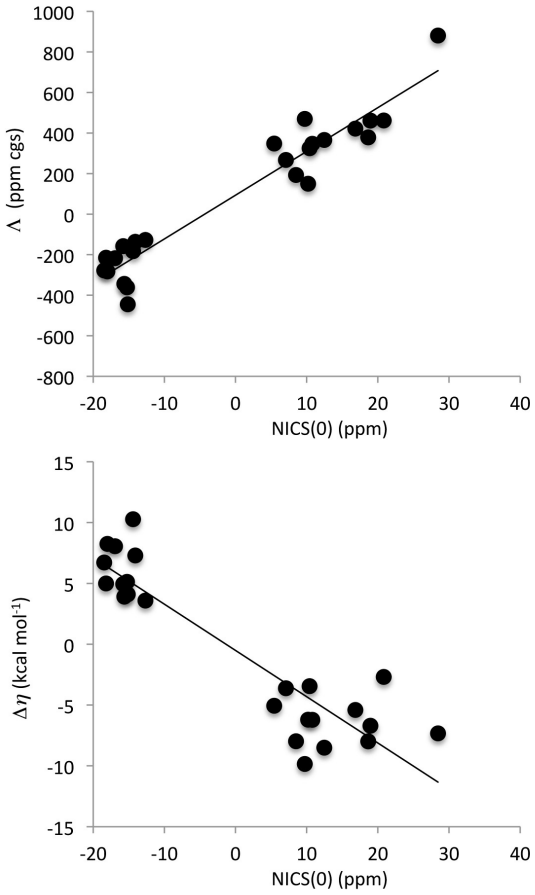

Fig. 9 Plot of the magnetic susceptibility exaltation (Λ) and the relative hardness ($\Delta\eta$) *versus* the isotropic NICS(0) values for octaphyrins.

Also bad correlations are found for the structural HOMA index. Although HOMA predicts correctly that the Möbius structures exhibit larger bond-equalization than Hückel structures in [36]octaphyrins, the differences in the HOMA values between aromatic and antiaromatic conformations is very small, ranging from 0.71 to 0.85. Therefore, the energetic ISE_{corr} and structural HOMA indices should be applied with caution in octaphyrins, and we strongly recommend to use the $\Delta\eta$, Λ and NICS-based indices to quantify the aromaticity of octaphyrins.

Having understood the structure-aromaticity relationships, we finally investigated the relationship between the NLO properties, aromaticity and the molecular topology of octaphyrins. Although the theoretical study on NLO properties of octaphyrins has not been performed yet, we have used the two-photon absorption (TPA) cross-sections values measured experimentally for neutral and diprotonated [36] and [38]octaphyrins.[28] As shown in Fig. 10, the NLO properties of the different octaphyrins are intrinsically related to their aromatic and structural properties. The lowest TPA cross-section value (σ_{TPA} = 800 GM) corresponds to the neutral [36]octaphyrin, which adopts a non-aromatic figure-eight conformation. Much larger two photon absorption cross-section value was reported for diprotonated [36]octaphyrin (σ_{TPA} = 5100 GM).[28] In that case, the preference for a Möbius topology together with the enhanced aromaticity upon protonation explains the much larger NLO properties of diprotonated species.

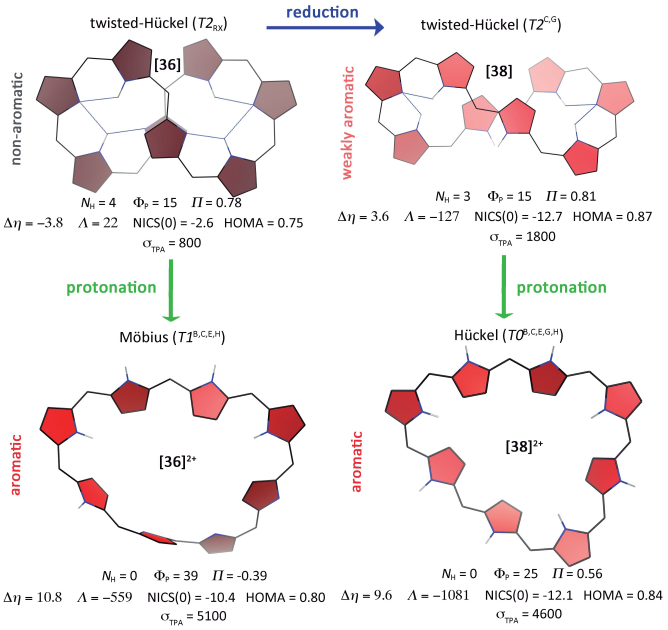

Fig. 10 Conformational and aromaticity changes of the octaphyrin macrocycle upon reduction and protonation. The structural and aromaticity descriptors are shown together with the TPA cross-section values (in GM).

A similar situation is found in [38]octaphyrins, in which the formation of a Hückel aromatic structure upon protonation is accompanied by a large increase of the TPA cross-section. By contrast, the figure-eight conformation, predicted to be the most stable for neutral [38]octaphyrin, is only weakly aromatic, leading to a σ_{TPA} = 1800 GM. Again, the presence of a moderate diatropic ring current in the twisted-Hückel conformation with [38] π-electrons explain the enhanced σ_{TPA} relative to the non-aromatic [36]counterpart. Accordingly, octaphyrins with greater aromatic character give rise to higher TPA cross-section values. Therefore, aromaticity provides a guiding principle for highly efficient two-photon absorption materials from expanded porphyrins. In fact, a large correlation is found between the experimentally determined TPA cross-section values and the relative hardness (R^2 = 0.92, Fig. S35).

Conclusions

The conformational preferences and aromaticity of [36]octaphyrins have been investigated using DFT calculations,

analysing the influence the solvent, substituents and protonation on the conformation and properties of octaphyrins. In the neutral state, the non-aromatic figure-eight conformation is preferred over the aromatic Möbius topologies owing to its more effective intramolecular hydrogen-bonding interactions and reduced ring strain. The figure-eight conformation is particularly stable in [36]octaphyrins, explaining why most of octaphyrin derivatives reported so far take figure-of-eight conformations.

Different external *stimuli* for triggering a conformational/aromaticity switch in octaphyrins have been explored, including protonation and redox reactions. Whereas protonation induces a topology change from a figure-eight to a Möbius conformation, redox reactions induce aromaticity switches keeping a twisted-Hückel topology. The combination of reduction and protonation of the macrocycle results in a highly aromatic Hückel conformation.

The energetic, magnetic, reactivity and structural aromaticity indices reveal a close relationship between the molecular topology, the number of π-electrons and aromaticity. With [36] π-electrons, Möbius structures are highly aromatic, whereas Hückel conformations are strongly antiaromatic. The paratropicity in the twisted-Hückel topology is strongly reduced towards untwisted conformations. Importantly, the aromaticity of all conformations is totally reversed upon redox reactions, so Hückel structures becomes aromatic in [34] and [38]octaphyrins. By contrast, the (anti)aromaticity of all the conformations is considerably enhanced upon protonation. The aromaticity of octaphyrins is revealed best by the magnetic indices (Λ and NICS) and the relative hardness rather than the structural and energetic descriptors.

Importantly, the NLO properties are greatly affected by the macrocyclic aromaticity of the π-electron system, as revealed by the correlations between the experimentally determined TPA cross-section values and the aromaticity indices. Since a drastic change in the aromaticity and NLO properties of the macrocycle is observed upon protonation and/or redox reactions, we conclude that [36]octaphyrins are promising platforms for the development of molecular switches for nanoelectronic applications.

From the methodological point of view, our DFT benchmark study showed that M06 predicts geometries for both Möbius and Hückel *meso*-octakis(pentafluorophenyl) [36]octaphyrins in better agreement with the XRD structures than standard functionals (PBE, BP86, B3LYP) and ωB97XD. However, M06 overestimates the stability of the twisted-Hückel topologies in diprotonated states. By contrast, B3LYP provides relative energies for diprotonated octaphyrins in good agreement with the experimental observations, although it describes the overall twisted-Hückel and Möbius structures worse. The discrepancies between both functionals mainly arise from an overestimation of the noncovalent interactions stabilizing the figure-eight topologies, such as the π-π staking interactions. Therefore, the selection of a functional for describing the thermochemistry of neutral and protonated octaphyrins is a complex task.

Acknowledgements

M. A. thanks the Fund for Scientific Research–Flanders (FWO-12F4416N) for a postdoctoral fellowship and the Free University of Brussels (VUB) for financial support. F. D. P and P. G. wish to acknowledge the VUB for a Strategic Research Program.

Notes and references

1 (*a*) P. J. Garratt, Aromaticity, John Wiley & Sons, New York, 1986; (*b*) V. I. Minkin, M. N. Glukhovtsev and B. Y. Simkin, Aromaticity and Antiaromaticity: Electronic and Structural Aspects, John Wiley & Sons, New York, 1994; (*c*) P. v. R. Schleyer, *Chem. Rev.*, 2001, **101**, 1115.

2 (*a*) Z. Chen and R. B. King, *Chem. Rev.,* 2005, **105**, 3613; (*b*) Q. Zhang, S. Yue, X. Lu, Z. Chen, R. Huang, L. Zheng and P. v. R. Schleyer, *J. Am. Chem. Soc.,* 2009, **131**, 9789; (*c*) M. J. Edward, *Coord. Chem. Rev.,* 2011, **255**, 2746; (*d*) I. Fernandez, G. Frenking and G. Merino*, Chem. Soc. Rev.,* 2015, **44**, 6452.

3 (*a*) A. Sergeeva, B. Averkiev and A. Boldyrev, *Struct. Bonding,* 2010, **136**, 275; (b) A. Boldyrev and L.S. Wang, *Chem. Rev.*, 2005, **105**, 3716; (*c*) J. M. Mercero, A. I. Boldyrev, G. Merino and J. M. Ugalde, *Chem. Soc. Rev.,* 2015, **44**, 6519.

4 (*a*) A. Narita, X.-Y. Wang, X. Feng and K. Müllen, *Chem. Soc. Rev.,* 2015, **44**, 6616; (*b*) F. J. Martin-Martinez, S. Fias, G. Van Lier, F. De Proft and P. Geerlings, *Chem. Eur. J.*, 2012, **18**, 6183; (c) X. Lu and Z. Chen, *Chem. Rev.*, 2005, **105**, 3643.

5 (*a*) H. S. Rzepa, *Chem. Rev.* 2005, **105**, 3697; (*b*) R. Herges, *Chem. Rev.* 2006, **106**, 4820; (*c*) A. Osuka and S. Saito, *Chem. Commun.,* 2011, **47**, 4330; (*d)* M. Garcia-Borras, S. Osuna, J.M. Luis, M. Swart and M. Solà, *Chem. Soc. Rev.* 2015, **43**, 5089; (*e*) P.v.R. Schleyer, J.I. Wu, F.P. Cossio and I. Fernández, *Chem. Soc. Rev.* 2015, **43**, 4909.

6 (*a*) A. Stanger, *Chem. Commun.,* 2009, 1939; (*b*) G. Frenking and A. Krapp, *J. Comput. Chem.*, 2007, **28**, 15; (*c*) P. v. R. Schleyer, *Chem. Rev.*, 2005, **105**, 3433; (*d*) R. Hoffman, *American Scientist*, 2015.

7 E. Heilbronner, *Tetrahedron Lett.,* 1964, **5**, 1923.

8 D. Ajami, O. Oeckler, A. Simon and R. Herges, *Nature*, 2003, **426**, 819.

9 Z. S. Yoon, A. Osuka and D. Kim, *Nature Chem*., 2009, **1**, 113.

10 (*a*) S. Saito and A. Osuka, *Angew. Chem. Int. Ed.*, 2011, **50**, 4342; (*b*) M. Alonso, B. Pinter, P. Geerlings and F. De Proft, *Chem. Eur. J.*, 2015, **21**, 17631.

11 M. Stępień, N. Sprutta and L. Latos-Grażyński, *Angew. Chem. Int. Ed.*, 2011, **50,** 4288.

12 (*a*) A. Osuka and S. Saito, *Chem. Commun.,* 2011, **47**, 4330; (*b*) Z. S. Yoon, D.-G. Cho, K. S. Kim, J. L. Sessler and D. Kim, *J. Am. Chem. Soc.*, 2008, **130**, 6930; (*c*) M.-C. Yoon, S. Cho, M. Suzuki, A. Osuka and D. Kim, *J. Am. Chem. Soc.*, 2009, **131**, 7360; (*d*) S. Cho, Z. S. Yoon, K. S. Kim, M.-C. Yoon, D.-G. Cho, J. L. Sessler and D. Kim, *J. Phys. Chem. Lett.*, 2010, **1**, 895; (*e*) M. Torrent-Sucarrat, J. M. Anglada and J. M. Luis, *J. Chem. Phys.*, 2012, **137**, 184306.

13 J. Y. Shin, K. S. Kim, M. C. Yoon, J. M. Lim, Z. S. Yoon, A. Osuka and D. Kim, *Chem. Soc. Rev,*, 2010, **39**, 2751.

14 Y. M. Sung, M.-C. Yoon, J. M. Lim, H. Rath, K. Naoda, A. Osuka and D. Kim, *Nature Chem.*, 2015, **7**, 418.

15 S. M. Rappaport and H. S. Rzepa, *J. Am. Chem. Soc.*, 2008, **130**, 7613.

16 (a) M. Solà, F. Feixas, J. O. C. Jiménez-Halla, E. Matito and J. Poater, *Symmetry*, 2010, **2**, 1156; (*b*) M. Alonso and B. Herradón, *Phys. Chem. Chem. Phys.*, 2010, **12**, 1305; (*c*) M. K. Cyrański, T. M. Krygowski, A. R. Katritzky and P. v. R.

Schleyer, *J. Org. Chem.*, 2002, **67**, 1333; (*d*) D. Ajami, K. Hess, F. Köhler, C. Näther, O. Oeckler, A. Simon, C. Yamamoto, Y. Okamoto and R. Herges, *Chem. Eur. J.*, 2006, **12**, 5434; (*e*) M. Alonso and B. Herradón, *J. Comput. Chem.*, 2009, **31**, 917.

17 J. I. Wu, I. Fernández and P. v. R. Schleyer, *J. Am. Chem. Soc.*, 2012, **135**, 315.

18 M. Alonso, P. Geerlings and F. De Proft, *Chem. Eur. J.*, 2012, **18**, 10916.

19 (*a*) P. v. R. Schleyer and F. Pühlhofer, *Org. Lett.*, 2002, **4**, 2873; (*b*) C. S. Wannere, P. v. R. Schleyer, *Org. Lett.* 2003, **5**, 865; (*c*) C. S. Wannere, D. Moran, N. L. Allinger, B. A. Hess, L.-J. Schaad and P. v. R. Schleyer, *Org. Lett.* 2003, **5**, 2983.

20 (*a*) M. Alonso, P. Geerlings and F. De Proft, *J. Org. Chem.*, 2013, **78**, 4419; (*b*) M. Alonso, P. Geerlings and F. De Proft, *Phys. Chem. Chem. Phys.* 2014, **16**, 14396.

21 M. Alonso, P. Geerlings and F. De Proft, *Chem. Eur. J.*, 2013, **19**, 1617.

22 (*a*) M. Stępień, L. Latos-Grażyński, N. Sprutta, P. Chwalisz and L. Szterenberg, *Angew. Chem. Int. Ed.*, 2007, **46**, 7869; (*b*) M. Stępień, B. Szyszko and L. Latos-Grażyński, *J. Am. Chem. Soc.* 2010, **132**, 3140; (*c*) B. Szyszko, N. Sprutta, P. Chwalisz, M. Stępień and L. Latos-Grażyński, *Chem. Eur. J.*, 2014, **20**, 1985.

23 (*a*) S. Saito, J. Y. Shin, J. M. Lim, K. S. Kim, D. Kim and A. Osuka, *Angew. Chem. Int. Ed.,* 2008, **47**, 9657; (*b*) J.-Y Shin, J. M Lim, Z. S. Yoon, K. S. Kim, M.-C Yoon, S. Hiroto, H. Shinokubo, S. Shimizu, A. Osuka and D. Kim, *J. Phys. Chem. B*, **2009**, *113*, 5794, (*c*) G. Karthik, J. Min Lim, A. Srinivasan, C. H. Suresh, D. Kim and T.K. Chandrashekar, *Chem. Eur. J.*, 2013, **19**, 17011.

24 M. C. Yoon, J. Y. Shin, J. M. Lim, S. Saito, T. Yoneda, A. Osuka and D. Kim, *Chem. Eur. J.,* 2011, **17**, 6707.

25 (*a*) M. Inoue and A. Osuka, *Angew. Chem. Int. Ed.* **2010**, *49*, 9488; (*b*) T. K. Ahn, J. H. Kwon, D. Y. Kim, D. W. Cho, D. H. Jeong, S. K. Kim, M. Suzuki, S. Shimizu, A. Osuka and D. Kim, *J. Am. Chem. Soc.*, **2005**, 127, 12856; (*c*) J. K Park, Z. S. Yoon, M.-C. Yoon, K. S. Kim, S. Mori, J.-Y. Shin, A. Osuka and D. Kim, *J. Am. Chem. Soc.*, 2008**, 130**, 1824.

26 Y. Shin, H. Furuta, K. Yoza, S. Igarashi and A. Osuka, *J. Am. Chem. Soc.*, 2001, **123**, 7190.

27 (*a*) L. Latos-Grażyński, *Angew. Chem. Int. Ed.*, 2004, **43**, 5124; (*b*) Y. Tanaka, S. Saito, S. Mori, N. Aratani, H. Shinokubo, N. Shibata, Y. Higuchi, Z. S. Yoon, K. S. Kim, S. B. Noh, J. K. Park, D. Kim and A. Osuka, *Angew. Chem. Int. Ed.*, 2008, **47**, 681; (*c*) Y. Tanaka, H. Shinokubo, Y. Yoshimura and A. Osuka, *Chem. Eur. J.*, 2009, **15**, 5674

28 J. M. Lim, J.-Y. Shin, Y. Tanaka, S. Saito, A. Osuka and D. Kim, *J. Am. Chem. Soc.*, 2010, **132**, 3105.

29 Gaussian 09, Revision B.01, M. J. Frisch, G. W. Trucks, H. B. Schlegel, G. E. Scuseria, M. A. Robb, J. R. Cheeseman, G. Scalmani, V. Barone, B. Mennucci, G. A. Petersson, H. Nakatsuji, M. Caricato, X. Li, H. P. Hratchian, A. F. Izmaylov, J. Bloino, G. Zheng, J. L. Sonnenberg, M. Hada, M. Ehara, K. Toyota, R. Fukuda, J. Hasegawa, M. Ishida, T. Nakajima, Y. Honda, O. Kitao, H. Nakai, T. Vreven, J. A. Montgomery, Jr., J. E. Peralta, F. Ogliaro, M. Bearpark, J. J. Heyd, E. Brothers, K. N. Kudin, V. N. Staroverov, T. Keith, R. Kobayashi, J. Normand, K. Raghavachari, A. Rendell, J. C. Burant, S. S. Iyengar, J. Tomasi, M. Cossi, N. Rega, J. M. Millam, M. Klene, J. E. Knox, J. B. Cross, V. Bakken, C. Adamo, J. Jaramillo, R. Gomperts, R. E. Stratmann, O. Yazyev, A. J. Austin, R. Cammi, C. Pomelli, J. W. Ochterski, R. L. Martin, K. Morokuma, V. G. Zakrzewski, G. A. Voth, P. Salvador, J. J. Dannenberg, S. Dapprich, A. D. Daniels, O. Farkas, J. B. Foresman, J. V. Ortiz, J. Cioslowski, D. J. Fox, Gaussian, Inc., Wallingford CT, 2010.

30 Y. Zhao and D. G. Truhlar, *Theor. Chem. Acc.*, 2008, **120**, 215.

31 For a detailed account on these types of basis sets, see: W. J. Hehre, L. Radom, P. v. R. Schleyer and J. A. Pople, *Ab Initio Molecular Orbital Theory*, Wiley, New York, 1986.

32 A. V. Marenich, C. J. Cramer and D. G. Truhlar, *J. Phys. Chem. B,* 2009, **113**, 6378.

33 (*a*) J. Kruszewski and T. M. Krygowski, *Tetrahedron Lett.*, 1972, **13**, 3839; (*b*) T. M. Krygowski, *J. Chem. Inf. Comput. Sci.*, 1993, **33**, 70; (*c*) T. M. Krygowski, H. Szatylowicz, O. A. Stasyuk, J. Dominikowska and M. Palusiak, *Chem. Soc. Rev.*, 2014, **114**, 6383.

34 (*a*) F. Sondheimer, R. Wolovsky and Y. Amiel, *J. Am. Chem. Soc.*, 1962, **84**, 274; (*b*) E. Vogel, *Pure Appl. Chem.*, 1993, **65**, 143.

35 H. J. Dauben, J. D. Wilson and J. L. Layti, *J. Am. Chem. Soc.*, 1968, **90**, 811.

36 F. De Proft and P. Geerlings, *Phys. Chem. Chem. Phys.*, 2004, **6**, 242.

37 T. A. Keith and R. F. W. Bader, *Chem. Phys. Lett.*, 1993, **210**, 223.

38 K. Wolinski, J. F. Hinton and P. Pulay, *J. Am. Chem. Soc.*, 1990, **112**, 8251.

39 (*a*) P. v. R. Schleyer, C. Maerker, A. Dransfeld, H. J. Jiao and N. Hommes, *J. Am. Chem. Soc.* 1996, **118**, 6317; (*b*) Z. Chen, C. S. Wannere, C. Corminboeuf, R. Puchta and P. v. R. Schleyer, *Chem. Rev.,* 2005, **105**, 3842; (*c*) H. F.-B. Shaidaei, C. S. Wannere, C. Corminboeuf, R. Puchta and P. v. R. Schleyer, *Org. Lett.*, 2006, **8**, 863.

40 E. R. Johnson, S. Keinan, P. Mori-Sánchez, J. Contreras-García, A. J. Cohen and W. Yang, *J. Am. Chem. Soc.*, 2010, **132**, 6498.

41 J. Contreras-García, E. R. Johnson, S. Keinan, R. Chaudret, J.-P. Piquemal, D. N. Beratan and W. Yang, *J. Chem. Theory Comput.*, 2011, **7**, 625.

42 A. D. Becke, *J. Chem. Phys.*, 1993, **98**, 5648.

43 J. P. Perdew, K. Burke and M. Ernzerhof, *Phys. Rev. Lett.*, 1997, **78**, 1396.

44 J.-D. Chai and M. Head-Gordon, *Phys. Chem. Chem. Phys.*, 2008, **10**, 6615.

45 (*a*) S. Grimme, *J. Comput. Chem.*, 2004, **25**, 1463S; (*b*) Ehrlich, J. Moellmann and S. Grimme, *Acc. Chem. Res.*, 2012, **46**, 916.

46 (*a*) A. D. Becke, *Phys. Rev. A* 1988, **38**, 3098; (*b*) J. P. Perdew, *Phys. Rev. B*, 1986, **33**, 8822.,

47 T. Yoneda, Y. M. Sung, J. M. Lim, D. Kim and A. Osuka, *Angew. Chem. Int. Ed.*, 2014, **53**, 13169.

48 G.R. Schaller, F. Topic, K. Rissanen, Y. Okamoto, J. Shen and R. Herges, *Nature Chem.*, 2014, **6**, 608.

49 M. Toganoh and H. Furuta, *J. Org. Chem.*, 2013, **78**, 9317.

50 J. R. Lane, J. Contreras-García, J. P. Piquemal, B. J. Miller and H. G. Kjaergaard, *J. Chem. Theory Comput.,* 2013, **9**, 3263.

51 (*a*) M. Suzuki and A. Osuka, *Chem. Eur. J.*, 2007, **13**, 196, (*b*) S. Shimizu, N. Aratani and A. Osuka, *Chem. Eur. J.*, 2006, **12,** 4909.

52 E. Marcos, J. M. Anglada and M. Torrent-Sucarrat, *J. Org. Chem.*, 2014, **79**, 5036.

53 S. Shimizu, J.-Y. Shin, H. Furuta, R. Ismael and A. Osuka, *Angew. Chem. Int. Ed.*, **2003**, 42, 78.

54 (*a*) F. Feixas, M. Solà and M. Swart, *Can. J. Chem.*, 2009, **87**, 1063; (*b*) F. Feixas, E. Matito, J. Poater and M. Solà, *Chem. Soc. Rev.*, 2015, **44**, 6434.

55 Recently, a new method to evaluate the strength and pathways of the magnetically-induced currents has been developed and applied to twisted hexaphyrins: (*a*) H. Fliegl, D. Sundholm, S. Taubert and F. Pichierri, *J. Phys. Chem. A* **2010**, *114*, 7153; (*b*) H. Fliegl, S. Taubert, O. Lehtonen and D. Sundholm, *Phys. Chem. Chem. Phys.*, 2011, **13**, 20500.

56 (*a*) P. Lazzeretti, *Prog. Nucl. Magn. Reson. Spectrosc.*, 2000*,* **36***,* 1; (*b*) P. Lazzeretti, *Phys. Chem. Chem. Phys.*, 2004, **6**, 217; (*c*) S. Pelloni and P. Lazzeretti, *J. Phys. Chem. A*, 2013*,* **117**, 9083; (*d*) G. Monaco and R. Zanasi, *J. Phys. Chem. A*, 2014*,* **118**, 1673.